Hydrol. Earth Syst. Sci., 17, 2981–3004, 2013
www.hydrol-earth-syst-sci.net/17/2981/2013/
doi:10.5194/hess-17-2981-2013

Hydrology and Earth System Sciences
Open Access

Hortonian runoff closure relations for geomorphologic response units: evaluation against field data

E. Vannametee, D. Karssenberg, M. R. Hendriks, and M. F. P. Bierkens

Department of Physical Geography, Faculty of Geosciences, Utrecht University, P.O. Box 80115, 3508 TC Utrecht, the Netherlands

Correspondence to: E. Vannametee (e.vannametee@uu.nl)

Received: 23 January 2013 – Published in Hydrol. Earth Syst. Sci. Discuss.: 6 February 2013
Revised: 28 May 2013 – Accepted: 18 June 2013 – Published: 26 July 2013

Abstract. This paper presents an evaluation of the closure relation for Hortonian runoff, proposed in Vannametee et al. (2012), that incorporates a scaling component to explicitly account for the process heterogeneity and scale effects in runoff generation for the real-world case studies. We applied the closure relation, which was embedded in an event-based lumped rainfall–runoff model, to a 15 km^2 catchment in the French Alps. The catchment was disaggregated into a number of landform units, referred to as Geomorphologic Response Units (GRUs), to each of which the closure relation was applied. The scaling component in the closure relation was identified using the empirical relations between rainstorm characteristics, geometry, and local-scale measurable properties of the GRUs. Evaluation of the closure relation performance against the observed discharge shows that the hydrograph and discharge volume were quite satisfactorily simulated even without calibration. Performance of the closure relation can be mainly attributed to the use of scaling component, as it is shown that our closure relation outperforms a benchmark closure relation that lacks this scaling component. The discharge prediction is significantly improved when the closure relation is calibrated against the observed discharge, resulting in local-scale GRU-properties optimal for the predictions. Calibration was done by changing one local-scale observable, i.e. hydraulic conductivity (K_s), using a single pre-factor for the entire catchment. It is shown that the calibrated K_s values are somewhat comparable to the observed K_s values at a local scale in the study catchment. These results suggest that, in the absence of discharge observations, reasonable estimates of catchment-scale runoff responses can possibly be achieved with the observations at the sub-GRU (i.e. plot) scale. Our study provides a platform for the future development of low-dimensional, semi-distributed, physically based discharge models in ungauged catchments.

1 Introduction

Lumped precipitation-runoff models represent a region, mostly a catchment, as a single unit. Larger watersheds are often disaggregated into a number of regions (e.g. sub-catchments, hillslopes, functional units, and so on), to which a series of such lumped models representing processes for particular hydrological compartments, such as the unsaturated zone, the groundwater zone, or the surface water zone, that are specifically defined for these regions are applied (i.e. a semi-distributed model). At the core of a lumped modelling approach lie the closure relations, which quantify the mass exchange fluxes between the hydrological compartments in the regions (Beven, 2006). A wide range of approaches exist for lumped modelling, including conceptual modelling approaches, mostly referred to as Hydrological Response Unit models (HRUs) (Flügel, 1995), and physically based approaches of which the most widely known is the Representative Elementary Watershed framework (Reggiani et al., 1998, 1999).

As with any hydrological modelling, the key challenge in lumped precipitation-runoff modelling is the identification of appropriate closure relations and estimation of parameter values used in the closure relations. A number of studies are dedicated to developing the closure relations for specific hydrological compartments that partly resolve the problems related to scale-dependent effects, process non-linearity,

sub-unit heterogeneity, and hysteresis (e.g. Lee et al., 2007; Reggiani and Rientjes, 2010; Troch, 2003; Vannametee et al., 2012). The existing closure schemes require parameter values that are representative for the region that is lumped by the model, which typically has a size above $10^5\,m^2$ (e.g. Fenicia et al., 2005; Varado et al., 2006). Direct measurement of lumped parameter values representative to this scale is notably difficult or even almost not possible (Mileham et al., 2008; Molnár and Julien, 2000; van Schaik et al., 2010), although remote sensing techniques might provide this possibility in the near future (Lakshmi, 2013; Vereecken et al., 2008). The alternative is to upscale the measured parameter values at local (point) scale to the values representative at the scale of the region modelled by the closure relations. This comes, however, with massive challenges and difficulties (Bierkens et al., 2000; Jana and Mohanty, 2012; McIntyre, 2012; Zehe et al., 2006). For instance, in Hortonian runoff modelling, which is the focus of this paper, derivation of the scale-transfer functions for saturated hydraulic conductivity was shown to be relatively difficult as the infiltration and runoff flux are strongly dependent on both the size of the region and the spatial variation over the region (Karssenberg, 2006). Due to these problems, parameter values in lumped catchment models are often derived by ad hoc calibration, mostly against catchment discharge (e.g. Betrie et al., 2011; Lazzarotto et al., 2006; Mango et al., 2011; Setegn et al., 2009). This has the major disadvantage, however, that derived parameter values cannot easily be transferred to other catchments because representative parameter values will change with unit geometry, spatial heterogeneity and boundary conditions (Beven, 2006; Blöschl and Sivapalan, 1995).

To address the issues discussed above, Vannametee et al. (2012) defined a rigorous approach for identifying the closure relations in lumped precipitation-runoff models, focussing on the closure relations related to Hortonian runoff, in particular the infiltration flux to the unsaturated zone, and the runoff flux. Their closure relations use local-scale parameter values as inputs to derive the runoff flux generated at the scale of the modelling units. To account for scale transfer, their closure relation explicitly includes scaling parameters, that are used to characterise the effects of geometry and process variability in the modelling units for Hortonian runoff generation. To avoid ad hoc estimation of these scaling parameters, Vannametee et al. (2012) provided a parameter estimation scheme, which is based on empirical relations between the geometry, and locally observable properties of the modelling units, including boundary conditions and past trajectory of surface water storage. These relations were identified from an extensive set of precipitation–runoff responses generated by a distributed, physically based, high-resolution model. It was shown that their closure relation could potentially lead to the modelling of Hortonian runoff by using a lumped model with input parameters representative at a local scale. They suggested using the units (or catchments) with uniform properties to allow imposing a number of assumptions essential in their formulation of the closure relation. The methodology proposed in Vannametee et al. (2012) is somewhat similar to the works by Massuel et al. (2011), in which they scaled up the surface runoff processes, using the detailed fine-scale, physically based model to derive the runoff coefficient as a basis to estimate the groundwater recharge over a large region.

In Vannametee et al. (2012), the closure relation was only tested for hypothetic watersheds using a synthetic data set of rainfall–runoff responses from the virtual experiments; thus questions regarding the transferability and applicability of closure relations in real-world situations remain to be investigated. Here, as the next logical step, we evaluate the performance of the closure relation developed by Vannametee et al. (2012), using a new discharge data set observed in a real catchment. Also, we investigate the improvement of the model's predictive capability as a result of the use of scaling parameters by a comparison of the model results with a closure relation that does not incorporate scaling parameters (i.e. as a benchmark). We specifically address the following research questions: (1) how suitable are the closure relations as proposed in Vannametee et al. (2012) for simulating observed catchment-scale hydrologic responses (i.e. hydrograph and total discharge volume)? (2) What are the advantages of using closure relations to represent processes within the modelling units over using a simple lumped rainfall–runoff model that neglects these processes?

The closure relations were applied to a small test catchment in the French Alps. Our modelling units are Geomorphologic Response Units (GRUs) that result from a geomorphological classification of the terrain into landform units. GRUs represent areas that are internally relatively homogenous, thus allowing us to use a set of uniform (i.e. lumped) parameters to describe the averaged unit characteristics. The catchment was disaggregated into a number of GRUs. The closure relations, including the scaling parameters, were parameterized for individual GRUs using properties (e.g. geometry, local-scale saturated hydraulic conductivity) and rainstorm characteristics observed in the field. Discharge was simulated for individual GRUs and subsequently routed over the drainage network. Performance of the closure relation was evaluated for two situations; in an ungauged and gauged basin. In the first situation, discharge was simulated using closure relations that were not calibrated and by using locally observed GRU properties or values reported in literature. For the gauged situation, on the other hand, closure relations were calibrated against the observed discharge to derive a local-scale input optimal for discharge simulation, as this local-scale parameter is often obtained with a large degree of uncertainty. It is important to note here that we did not calibrate the scaling parameters or modify the relations used to determine the scaling parameters, as this is considered to be part of the closure relation itself that also needs to be evaluated.

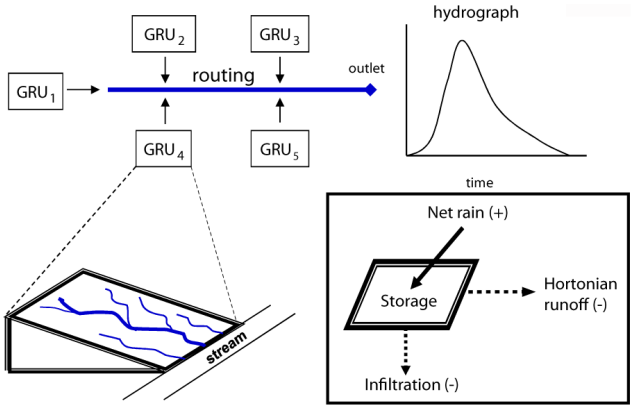

Fig. 1. Schematic representation of the modelling framework used in the study. The Hortonian runoff generating processes for individual GRUs defined in the closure relation are shown in concept in the box. The plus and minus signs indicate incoming and outgoing fluxes of the GRUs, respectively.

The paper is organised in three parts. The first part describes the methodology and the application of closure relations in the test catchment. In the second part we present the evaluation results and performance for both types of closure relations (i.e. with and without scaling parameters). In the last section, we analyse and discuss the predictive performance, and assess the improvements gained from using the closure relations with scaling parameters.

2 Methodology

2.1 Catchment-scale rainfall–runoff modelling framework

The modelling framework has four model components, which can be combined into two main modules – the module for calculating boundary conditions (i.e. net rainfall) and the module for runoff modelling. The runoff module consists of the closure relations simulating the Hortonian runoff flux generated from GRUs and a routing component to obtain the runoff response at the catchment outlet (Fig. 1). At the GRU scale, runoff generation is simulated using two approaches. One approach uses the closure relation proposed by Vannametee et al. (2012). As a benchmark we use another closure relation that does not include scaling parameters. The simulation is done over time t, using a time step (Δt) of 5 min for all components. Below, the symbols used in the equations represent properties at an individual GRU, except if indicated otherwise. If properties of multiple GRUs are presented in the same equation, the subscript i is used to indicate properties of each individual GRU$_i$.

2.1.1 Mass-balance closure relations for a Geomorphologic Response Unit

Closure relations using the scaling parameters

A brief summary of the closure relation using the scaling parameters developed by Vannametee et al. (2012), denoted as C, is presented here. For each GRU, the change in the surface water storage S_t (m) of the Hortonian runoff zone (Lee et al., 2007) is modelled as

$$\frac{\mathrm{d}S_t}{\mathrm{d}t} = e_{\mathrm{ctop},t} - e_{\mathrm{cu},t} - e_{\mathrm{co,\,cr},t}. \quad (1)$$

In Eq. (1), t is time (h); $e_{\mathrm{ctop},t}$ (m h^{-1}) is the net rain flux at t; $e_{\mathrm{cu},t}$ (m h^{-1}) is the infiltration flux to the unsaturated zone at t; and $e_{\mathrm{co,cr},t}$ (m h^{-1}) is the outgoing runoff flux of the domain to the saturated overland flow and channel zones.

The proportion of the GRU where Hortonian runoff occurs changes over time. The GRU-scale infiltration flux is determined as a function of both water availability at the soil surface and the maximum infiltration capacity (i.e. potential infiltration rate), taking account of the runon-runoff process within the GRUs during a rain event. Using the Green & Ampt infiltration equation (Kale and Sahoo, 2011), the closure relation for the GRU-scale infiltration flux is defined as

$$e_{\mathrm{cu},t} = -\min\Big[\left(e_{\mathrm{ctop},t}\cdot\Delta t\right) + S_t, \rho_t \cdot K_{\mathrm{s}}\left(1+\frac{H_{\mathrm{f}}(\eta-\theta)}{F_t}\right)\cdot\Delta t\Big]/\Delta t. \quad (2)$$

In Eq. (2), "min[x, y]" selects the lesser value of x (i.e. the depth of water available for infiltration) and y (i.e. potential infiltration depth at t over the Hortonian runoff zone); ρ_t (-) is the ponding fraction at t, representing the proportion of the GRU with Hortonian runoff and infiltration; K_{s} (m h^{-1}) is the saturated hydraulic conductivity; H_{f} (m) is the matric suction at the wetting front; η (-) is the soil effective porosity; θ (-) is the antecedent moisture content; and F_t (m) is the cumulative infiltration at t. During the rainstorm, infiltrating water is supplied by rainwater and the infiltration flux is spatially uniform over the GRUs; the ponding fraction is assumed to be one. After the storm period, the infiltration flux becomes spatially variable and the extent of the Hortonian runoff zone (i.e. ponded area) decreases over time. This is related to the flow pattern that determines the spatial pattern of runoff in the GRUs (Vannametee et al., 2012). The ponding fraction is modelled as

$$\rho_t = a\cdot S_{t-\Delta t}; t \notin \boldsymbol{T} \quad = 1 \quad ; t \in \boldsymbol{T}, \quad (3)$$

where a (m^{-1}), the ponding factor, is a scaling parameter related to the spatial variation in runoff and infiltration; $\boldsymbol{T}$, a set of the time domain during which the GRUs receives rainwater. Note that rainstorms are modelled as distinct events in time.

Discharge from the GRU is simulated using a linear reservoir and related to surface storage. As hydrologic responses are not instantaneous, we use a past state of the GRU storage to calculate the responses at the time of interest, accounting for travel times over the slope. The Hortonian runoff flux leaving the GRU to the channel is, thus, modelled as

$$\begin{aligned} e_{\mathrm{co,\,cr},\,t} &= b \cdot S_{t-c}; t > c \\ &= 0 \qquad ; t \le c, \end{aligned} \tag{4}$$

and discharge from the GRU (Q_t; $\mathrm{m^3\,h^{-1}}$) is calculated as

$$Q_t = e_{\mathrm{co,\,cr},t} \cdot A. \tag{5}$$

In Eq. (4), b ($\mathrm{h^{-1}}$) is the reservoir parameter, a scaling parameter representing the storage properties of the GRU; c (h) is the third scaling parameter, a lag time representing the delay in GRU storage in releasing water; S_{t-c} (m) is the storage in the GRU, expressed as a depth of water layer at the surface at $t-c$; A ($\mathrm{m^2}$) is the area of the GRU.

The three scaling parameters (i.e. a, b, and c) can be directly estimated for each GRU from eight observable parameters. These are the rainstorm characteristics (i.e. average storm intensity R_{avg} ($\mathrm{m\,h^{-1}}$) and storm duration T (h)), average geometry of GRU (i.e. slope gradient s (-), slope length L (m), and micro relief c_1 (m)), and local-scale observable soil parameters within GRU (i.e. saturated hydraulic conductivity, matric suction at the wetting front, and initial moisture content). Following Vannametee et al. (2012), estimation of the value of these parameters is done by distance-weighted interpolation between points in a large database (approximately 65 000 scenarios) of these observable characteristics with associated scaling parameters.

Closure relations without scaling parameters

In order to evaluate the performance of the closure relation C, we use another closure relation, referred to as C^*, which has a form that is similar to C but without the scaling components. C^* is defined by using fixed values of the scaling parameters; $a = 0$ in Eq. (3) and $b = 1$, $c = 0$ in Eq. (4). This results in a closure relation that does not take into account the scaling effects and spatial processes in runoff generation. By defining $b = 1$, C^* neglects storage within the GRU, which results in instantaneous runoff response from the GRU (i.e. $c = 0$). Without this storage capacity, the past state of the GRU storage, $S_{t-\Delta t}$ (Eq. 3) is zero, which results in a zero value for the ponding fraction ρ_t. Thus, infiltration after a rain event is neglected (i.e. $a = 0$). The outgoing runoff flux at t is simply a surplus of the net rain flux at t after abstracting the infiltration flux at t:

$$e^*_{\mathrm{co,\,cr},t} = e_{\mathrm{ctop},t} + e^*_{\mathrm{cu},t}. \tag{6}$$

The superscript * indicates that the fluxes are calculated from the closure relation C^*. In Eq. (6), multiplication of $e^*_{\mathrm{co,\,cr},t}$ by the area of the GRUs results in the discharge of the GRUs (i.e. Eq. 5). Without storage capacity, the infiltration flux in Eq.3 is reduced to

$$\begin{aligned} e^*_{\mathrm{cu},t} &= -\min\left[e_{\mathrm{ctop},t}, K_{\mathrm{s}}\left(1 + \frac{H_{\mathrm{f}}(\eta-\theta)}{F_t}\right)\right]; t \in \boldsymbol{T} \\ &= 0 \qquad\qquad\qquad\qquad\qquad\qquad ; t \notin \boldsymbol{T}. \end{aligned} \tag{7}$$

2.1.2 Runoff generation at the catchment level

Discharge Q_t generated from each GRU is assumed to flow directly to the channel network, which drains water to the outflow point of the catchment. We assume no gain or loss of water in the channel zone by other processes (i.e. channel precipitation, infiltration, and evaporation) because these amounts of water are relatively small compared to the amount of discharge volume generated from GRUs (i.e. the channel reaches are relatively short). The travel time C_i (h) of discharge from GRU_i to the catchment outlet is calculated as

$$C_i = \frac{D_i}{\left((A_{\mathrm{r}}/P)^{2/3} \cdot \sqrt{S_i} \cdot n^{-1}\right)}. \tag{8}$$

In Eq. (8), D_i (m) is the distance over the drainage network from the outlet of GRU_i to the catchment outlet. The denominator is the flow velocity ($\mathrm{m\,h^{-1}}$) along the channel, calculated using Manning's formula, with A_{r} ($\mathrm{m^2}$) the average channel cross section, P (m) the wetted perimeter, S_i (-) the averaged channel slope gradient along the flow path from the outlet of GRU_i to the catchment outlet, n ($\mathrm{h\,m^{-1/3}}$) the Manning's roughness coefficient of the channel.

The discharge at the catchment scale at t ($Q_{\mathrm{W},t}$; $\mathrm{m^3\,h^{-1}}$) can be derived as a sum of the discharges generated from all individual GRUs that reach the outlet at t:

$$Q_{\mathrm{W},t} = \sum_{i=1}^{N} Q_{i,t-C_i}, \tag{9}$$

where $Q_{i,t-C_i}$ is the discharge ($\mathrm{m^3\,h^{-1}}$) generated from GRU_i at $t - C_i$; N is the total number of GRUs.

2.1.3 Forcing and boundary conditions

Model forcing and boundary conditions required for the closure relations are net rain flux and antecedent moisture content before the events start, derived for individual GRUs. Since these components are not part of the closure relation for Hortonian runoff, description of these components is given in a separate section.

Net rain flux is defined as the rain flux that reaches the soil surface of the GRU after subtraction of the interception:

$$e_{\mathrm{ctop},t} = R_t - \min\left[(R_t \cdot v_{\mathrm{cov}}), \left(\frac{S_{\mathrm{I,\,max}} - S_{\mathrm{I},t-1}}{\Delta t}\right)\right] \tag{10}$$

$$v_{\mathrm{cov}} = e^{-k \cdot \mathrm{LAI}} \tag{11}$$

$$S_{\mathrm{I,\,max}} = \mathrm{LAI} \cdot S_{\mathrm{I,\,leaf}} \tag{12}$$

$$S_{\mathrm{I},t} = \min(S_{\mathrm{I,\,max}}, S_{\mathrm{I},t-1} + e_{\mathrm{ctop},t-1}). \tag{13}$$

In Eq. (10), R_t ($\mathrm{m\,h^{-1}}$) is the rain flux. The second term represents the interception, in which v_{cov} (-) is the vegetation cover, estimated by the Beer–Lambert equation (Bulcock and Jewitt, 2010), $S_{\mathrm{I,\,max}}$ (m) is the maximum content of the interception storage, and $S_{\mathrm{I},t}$ (m) is the actual interception storage. In Eqs. (11) and (12), k (-) is a light extinction coefficient, LAI (-) is the leaf area index, $S_{\mathrm{I,\,leaf}}$ (m) is the maximum storage capacity per unit leaf area. We assume no canopy loss during events. Furthermore, it is assumed that the rainwater intercepted by the canopy does not reach the soil surface and has completely evaporated after the event. The canopy interception storage is, thus, empty at the start of the following event.

As initial soil moisture content at the start of the events was not monitored in the field, a simple soil water balance model of the unsaturated zone is used to obtain the initial soil water content for an individual GRU at the start of the events. We assume large enough groundwater depth such that there is no influence of groundwater on the upper soil zone. Soil moisture content of individual GRUs at t (θ_t) is estimated by

$$\theta_t = \max\left[\min\left[\left(\frac{S_{\mathrm{rz},t} + R_t \cdot \Delta t - E_{\mathrm{a},t}}{r}\right), \theta_{\mathrm{s}}\right] \theta_{\mathrm{PWP}}\right], \tag{14}$$

where $S_{\mathrm{rz},t}$ (m) is the soil water in the root zone, r (m) the averaged root-zone depth of the catchment, $E_{\mathrm{a},t}$ (m) the actual evapotranspiration flux, θ_{s}(-) the soil moisture content at saturation, and θ_{PWP} (-) the soil moisture content at permanent wilting point. Note here that r, θ_{s}, and θ_{PWP} are assumed constant for all GRUs, and that θ_{s} equals soil porosity. The actual evapotranspiration can be estimated as a function of the potential evapotranspiration $E_{\mathrm{p},t}$ (m), soil water availability, and soil water stress (Xia and Shao, 2008):

$$\begin{aligned} E_{\mathrm{a},t} &= E_{\mathrm{p},t} \qquad\qquad ; k_{\theta,t} \geq k^*_{\theta} \\ &= E_{\mathrm{p},t} \cdot k_{\theta,t} \cdot \frac{1}{k^*_{\theta}} ; k_{\theta,t} < k^*_{\theta} \end{aligned} \tag{15}$$

$$k_{\theta,t} = \frac{\theta_t - \theta_{\mathrm{PWP}}}{\theta_{\mathrm{fc}} - \theta_{\mathrm{PWP}}}, \tag{16}$$

where $k_{\theta,t}$ (-) is the fraction of readily available water for plants in the root zone of the GRU. k^*_{θ} (-) is the critical threshold below which the soil is considered under water stress, commonly set at 0.5 or at a moisture content of half the soil moisture content at field capacity, θ_{fc} (-) (Dingman, 2002; Gervais et al., 2012). At this point, soil water availability for plants is limited and the actual evapotranspiration rate becomes less than the potential evapotranspiration (Pereira et al., 1999).

The potential evapotranspiration flux is assumed to be spatially uniform and calculated using a conceptual evapotranspiration model. We did not use a physically based evapotranspiration model (e.g. Penman–Monteith equation) because it has shown in Oudin et al. (2005) that the conceptual models provide sufficiently reliable estimates of evapotranspiration for a lumped model application. In setting up our model, we compared a number of different conceptual evapotranspiration models, namely; Thornthwaite, Hamon, Blaney–Criddle, and Romanenko (Xu and Singh, 2001). The results show that estimates of potential evapotranspiration using these models are relatively comparable. The difference in monthly evapotranspiration is between 20–40 mm, with a maximum of 75 mm in summer. To represent the evapotranspiration in the study area (Sect. 2.2.1), we selected the Thornthwaite method because it calculated a yearly estimate of evapotranspiration that is close to that observed in the study catchment, which is $750\,\mathrm{mm\,yr^{-1}}$ (De Jonge, 2006) Monthly potential evapotranspiration using the Thornthwaite method is calculated as

$$E_{\mathrm{p}} = \frac{4}{3} \cdot \frac{N_m}{30} \cdot l_d \cdot \left(\frac{10 \cdot \overline{T_m}}{I_h}\right)^{\lambda} \tag{17}$$

$$I_h = \sum_{m=1}^{12} \left(\frac{\overline{T_m}}{5}\right)^{1.51} \tag{18}$$

$$\begin{aligned} \lambda = {} & 6.7 \times 10^{-7} \cdot I_h^3 - 7.7 \times 10^{-5} \cdot I_h^2 \\ & + 1.8 \times 10^{-2} \cdot I + 0.49, \end{aligned} \tag{19}$$

where N_m (days) is the number of days in a given month m; l_d(h) is the average monthly day length. I_h (°C) is an annual heat index; $\overline{T_m}$ (°C) is the mean monthly air temperature of a month m; λ is an empirical coefficient. Monthly $E_{\mathrm{p},t}$ obtained in Eq. (17) is equally distributed over each time step Δt and subsequently used to determine soil moisture content at GRUs in Eq. (14).

2.2 Catchment and observations

2.2.1 Description of the catchment

The catchment is a first-order sub-basin of the Buëch catchment, located near the village of Savournon in the administrative department of Hautes-Alpes, France. The catchment has a size of $15.7\,\mathrm{km^2}$ with an elevation range of 710–1780 m (Fig. 2). The region has a Mediterranean climate with Alpine influences (Van Steijn and Hétu, 1997). Lithology of the test catchment is characterised by deposits of Callovian–Oxfordian black marls, known as "Terres Noires" (Descroix and Gautier, 2002; Oostwoud Wijdenes and Ergenzinger, 1998; Giraud et al., 2009), which are found below the "Calcaire Tithonique" limestone. The morphology of the catchment is mainly shaped by periglacial processes during the Pleistocene. The upper part of the catchment is dominated by steep scree slopes below "Calcaire Tithonique" limestone hogbacks. Eroded materials from the upslope area

contribute to the formation of extensive fan-shape alluvial deposits at the flat part of the catchment, on which the major land use activities are pasture and agriculture. Intensive erosion on highly erodible marly deposits on the steep areas results in the formation of a badlands topography and deep-cut gullies (Mathys and Klotz, 2008). Vegetation characteristics in the catchment are quite variable, ranging from Mediterranean shrubs to a number of deciduous and alpine coniferous species.

2.2.2 Field data collection

Meteorology and discharge

A meteo station was installed approximately at the centre of the catchment. Temperature, air pressure, relative humidity, incoming solar radiation, wind speed and wind direction were recorded as an average state for 0.5 h intervals. Rainfall data were collected at 12 locations over the period of March to October 2010 (Fig. 2) by using tipping bucket rain gauges with a bucket volume representing 0.2 mm of rain.

Discharge data were collected at 3 locations (Fig. 2). Upstream areas (i.e. sub-catchments) above the gauging locations are 11.9, 3.8, and 0.6 km^2, referred to in this paper as a Large (L), Medium-sized (M) and Small (S) catchment, respectively (Fig. 3). L and M are independent from each other in terms of surface water because they are separate catchments, whereas S is a sub-catchment of M. The water stage at these locations was continuously recorded using pressure transducers. The stream bed and cross-sectional profile at the measurement location for the S catchment were fixed using the rectangular weir construction, while this construction was not used in the water stage measurement for L and M catchment. Stream discharge was measured 15–20 times at each location using salt dilution gauging with the slug injection method (Hendriks, 2010; Moore, 2004). Taking uncertainty in the measurements of water stage and discharge into account, a number of possible stage-discharge rating curves at each measurement location were constructed, from which an ensemble of discharge time series for 3 catchments were obtained accordingly. The final hydrograph for each catchment was calculated by averaging the hydrograph realizations that give the best-estimated discharge at the time measurements were done.

Although Hortonian the runoff process is the main focus in this study, it is not assumed that Hortonian runoff is the only runoff generating mechanism in our study catchment because groundwater flow also contributes to the stream. Thus, separation of the hydrograph is required to retrieve the Hortonian runoff component. This was done on an event basis using a graphical method (Hendriks, 2010). A straight line was projected from the start of the hydrograph rising to intersect the hydrograph at the falling limb, where the contribution of the Hortonian runoff to the event's discharge had ended. The partition of discharge above this straight line is considered as Hortonian runoff. The runoff partition point was indicated where the slope of the hydrograph or slope of the recession coefficient in the recession limb is inflected in the semi-logarithm plot (Blume et al., 2007). For reliable estimation of Hortonian runoff using this simple technique, we only focus on large rainstorm events that a significant amount of discharge was generated and hydrographs showed a clear rising and falling limb. In these events, Hortonian runoff (i.e. quick flow) can be clearly identified and partitioned from the base flow component. Moreover, if several inflection points were observed on the hydrograph recession limb, we selected the earliest point as a discharge separation point to ensure that the runoff component is mainly generated from the Horton process, which is the fast runoff generation mechanism.

Geomorphology, soil and vegetation

Topography, morphology of the landscape, geologic parent material, and characteristics of the sediment deposits at the surface and near surface were investigated throughout the catchment. Soil texture and regolith thickness were also estimated at a number of locations. The orientation of the hill slope relative to the channel network and catchment drainage system was also noted. These observations were used to map the landscape's geomorphic characteristics and resulted in the geomorphological map of the catchment (i.e. see Sect. 3.1).

Saturated hydraulic conductivity for each different regolith type was measured at a number of locations, covering an area of 100 km^2 that also includes the study catchment. The local scale K_s values were measured over a plot size of 30 cm × 30 cm, using rainfall simulation method (Adhikari et al., 2003). Artificial rain was generated from a pressure-controlled water reservoir containing a sprinkler head and a number of capillary tubes to release the water at the desired intensity. The amount of rainwater applied to the plot and corresponding generated runoff were measured every minute, from which the infiltration rate can be subsequently derived. The K_s value for each experimental plot was determined by curve fitting, in which the K_s value was chosen resulting in the best fit to the Green & Ampt infiltration curve (Kale and Sahoo, 2011).

Vegetation was observed and mapped as units of relatively uniform vegetation types (Fig. 3). For each vegetation unit, a number of plots with a size of 100 m^2 (i.e. 10–15 plots) was randomly chosen. The proportion of the area covered by vegetation in each plot was visually estimated and averaged to obtain a representative vegetation cover for each vegetation unit.

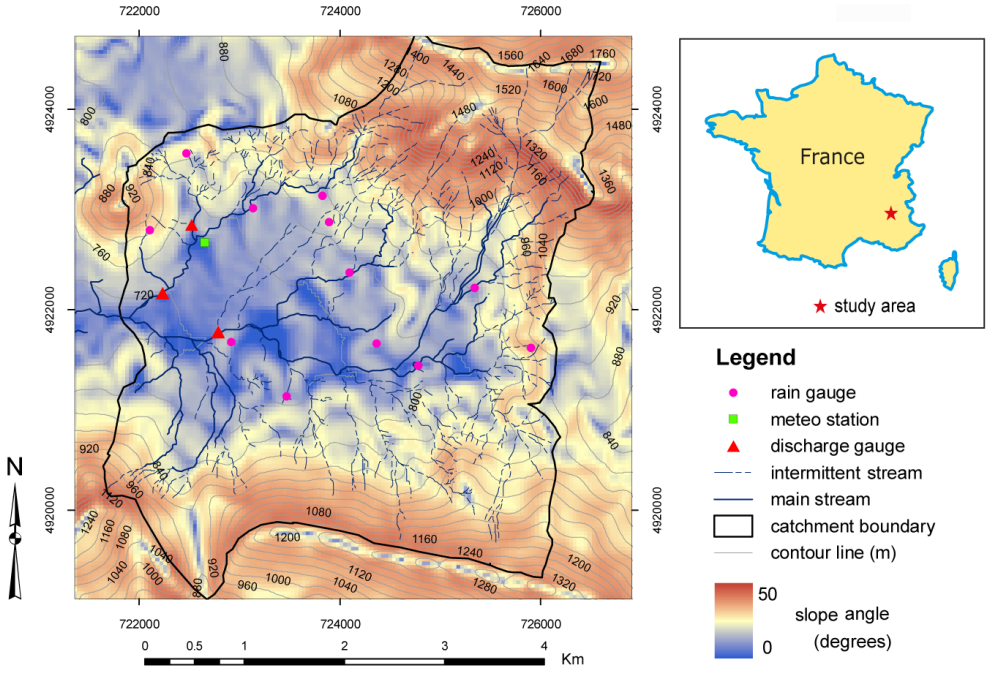

Fig. 2. Location and topographical characteristics of the study catchment, including the measurement locations of rainfall, meteo, and discharge data.

Delineation of the GRUs

Information on geomorphology, vegetation and the drainage network are crucial in the disaggregation of the study catchment into a number of GRUs. The GRUs were delineated such that the units are uniform in terms of genesis, structural pattern and hydrological properties. In this study, GRUs were derived by subdividing the major geomorphologic units into more fundamental landscape units with distinct vegetation and regolith properties. The boundaries of the units were defined by the local watershed divide or coincided with the channels to which the units drain. This delineation rule simplifies our case study by restricting the GRU's incoming flux only to the net rain. GRUs do not receive the cross-boundary surface runoff flux from adjacent GRUs (i.e. runon). Hydrologic properties and processes operating over individual GRUs can be regarded as relatively homogeneous.

2.3 Parameterization in the modelling framework

Forcing data, boundary conditions, and properties of individual GRUs were obtained from field observation or taken from various sources of reference. Details of the parameterization methods and parameter values used in the closure relations are presented in Table 1.

2.4 Sensitivity analysis

A sensitivity analysis was performed by calculating changes in hydrograph characteristics as a result of changes in model parameters. This was done for each model parameter separately, considering K_s, H_f, θ, LAI, $S_{I,leaf}$, and n. The model parameter was adjusted by $\pm 25\,\%$ of the value used for the base runs (i.e. values representing catchment characteristics derived from field data, Table 1). The relative changes in three hydrograph components; discharge volume, peak discharge, and time to peak discharge were calculated and averaged over all events used in the evaluation of the closure relation performance. The model sensitivity was investigated for the closure relation C and the benchmark closure relation C^*.

2.5 Calibration and evaluation of closure relations

For the scenarios with calibration of closure relations, calibration was performed by matching the simulation results to the observed discharge at each catchment outlet. We used a simple split-sample approach for the calibration. Two sets of events, in total approximately half of all events observed in each catchment, were randomly selected for calibration and validation. As we focus on the capacity of the closure relations to produce accurate discharge responses (i.e. the shape of hydrograph), the objective function used in the calibration is the Nash–Sutcliffe efficiency index, E (-):

$$E = 1 - \frac{\sum_{t=1}^{T_{end}} (Q_{t,sim} - Q_{t,obs})^2}{\sum_{t=1}^{T_{end}} (Q_{t,obs} - \overline{Q}_{obs})^2}, \quad (20)$$

Table 1. Input, parameters, and parameterization method used in the modelling framework.

Group	Symbol	Description	Spatial unit	Values/range	Methods/remarks
Rainfall	R_t	Rainfall flux ($m\,h^{-1}$)	GRU	–	Averaging a precipitation map over each GRU for each time step. Precipitation maps have grid cell sizes of 37.5 m^2, and are created by inverse distance interpolation of observed precipitation using an inverse distance exponent of two (Ahrens, 2006).
	R_{avg}	Event averaged rainfall intensity ($m\,h^{-1}$)	GRU	–	Calculated for the period that averaged rain depth over the GRUs is above 0.07 mm. This threshold is arbitrarily set to indicate the smallest rain depth that is recognised as an event.
	T	Event duration (h)	GRU	–	Sum of time steps that the averaged rain depth over the GRUs is above 0.07 mm
Climate	$\overline{T_m}$	Monthly averaged Temperature (°C)	Catchment	–	Measured in 0.5 h intervals and averaged on a monthly basis
	l_d	Monthly average day length (h)	Catchment	–	Sum of the daylight hours, estimated using the CBM model (Forsythe et al., 1995) over each month
Vegetation	LAI	Leaf area index (–)	GRU	0.01–10	Estimated for each vegetation unit using the LAI global data set (Scurlock et al., 2001). A surcharge of 2 was added to the forest-type units to compensate for the vegetation layer at the forest floor (Breuer et al., 2003). The average LAI for each vegetation unit was obtained by reducing the estimated LAI with a fraction of vegetation cover observed in the field.
	v_{cov}	Fraction of vegetation cover (–)	GRU	0.05–1	Field observation. Note that the vegetation cover fraction observed in the field was only used for deriving the average LAI of the vegetation units. For calculating interception and net rain flux, the vegetation cover fraction at the GRUs was estimated using Eq. (11).
	$S_{l,leaf}$	Maximum interception capacity per LAI (mm)	GRU	0.001–1.3	Estimated for each vegetation type using values suggested by Koivusalo et al. (2006) and Brolsma et al. (2010). A surcharge of 0.3 mm was added to the forest-type units to account for the additional interception capacity of the undergrowth at the forest floor.
	k	Light extinction coefficient (–)	Catchment	0.5	Brolsma et al. (2010); Kuriakose et al. (2009)
Soil	K_s	Saturated hydraulic conductivity ($m\,h^{-1}$)	GRU	–	Estimated from the GRU's regolith properties, which are related to the geomorphology. The referred-to values are reported in Rawls et al. (1982). See Table 4.
	H_f	Matric suction at the wetting front (m)	GRU	–	Estimated from the GRU's regolith properties, which are related to the geomorphology. The referred-to values are reported in Rawls et al. (1982). See Table 4.
	η	Porosity (–)	Catchment	0.42	Used value for the loamy soil, which is the average soil texture of the catchment (Rawls et al., 1982).
	θ	Moisture content at the start of simulation period (–)	Catchment	0.25	We used a slightly smaller value for the moisture content at field capacity for loamy soil (i.e. the average soil texture of the catchment) as the catchment was relatively dry at the start of the simulation period.
	θ_{PWP}	Moisture content at wilting point (–)	Catchment	0.1	Value used for loamy soil, which is the average soil texture of the catchment (Rawls et al., 1982).
	θ_{fc}	Moisture content at Field capacity (–)	Catchment	0.27	Value used for loamy soil, which is the average soil texture of the catchment (Rawls et al., 1982).
	k^*_θ	Critical moisture content (–)	Catchment	0.5	Dingman (2002); Gervais et al. (2012)
	r	Root zone depth (cm)	Catchment	50	Assumed
	c_1	Micro relief on GRU surface (mm)	GRU	80–0.4	Generated random fields of micro relief, using different values of c_1, for a hypothetical hill slope that has the same slope gradient for each GRU. We determined the drainage direction path over the GRUs by following the direction from a cell to the steepest descent as determined by its eight neighbouring cells (Burrough and McDonnell, 2004). We chose the c_1 value that results in a flow pattern most resembling that of the GRU observed in the field.
GRU Geometry	s	Slope gradient ($m\,m^{-1}$)	GRU	–	Extracted from the digital elevation data (DEM)
	L	Unit Length (m)	GRU	–	Calculated as a weighted average of the longest drainage paths from the GRU's divide to the GRU's outlets according to the upstream areas.
Channel	A_r	Channel cross section (m^2)	Sub-catchment	0.3 (L) 0.15 (M) 0.04 (S)	Field observation at a number of transects along stream channels. We calculated the average cross section for each sub-catchment.
	D_i	Distance from a GRU outlet to the (sub) catchment outlet (m)	GRU	–	Calculated from the local drainage direction (ldd) map
	S_i	Channel slope ($m\,m^{-1}$)	GRU	-	Averaged slope at each grid cell over the drainage path from a GRU outlet to the (sub)catchment outlet.
	n	Manning's coefficient ($h\,m^{-1/3}$)	Catchment	0.3	These estimations are based on the observed stream bed materials, using a value given in Chow et al. (1988)

where T_{end} is the end time of simulation; $Q_{t,sim}$ ($m^3\,h^{-1}$) is discharge simulated at t from the closure relations, $Q_{t,obs}$ ($m^3\,h^{-1}$) is the observed discharge at t; and $\overline{Q}_{obs}$ ($m^3\,h^{-1}$) is the mean observed discharge. This calibration procedure was used for the model using both closure relations C and C^*.

As we aim to evaluate the performance of closure relations proposed in Vannametee et al. (2012) including relations between the scaling parameters and measurable characteristics of a GRU, calibration is only allowed for the local-scale measurable parameters, which are usually obtained with a large degree of uncertainty. The saturated hydraulic conductivity

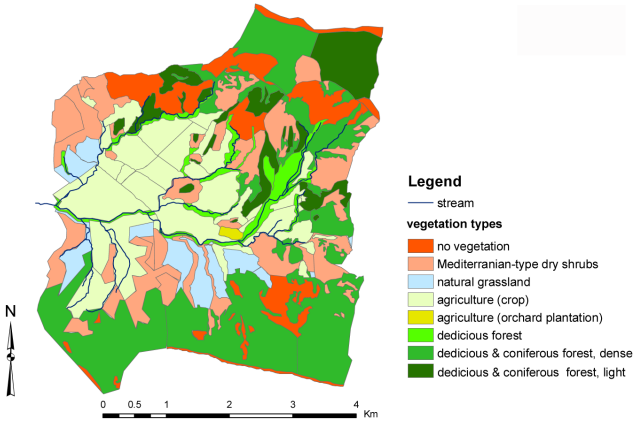

Fig. 3. Vegetation characteristics of the catchment.

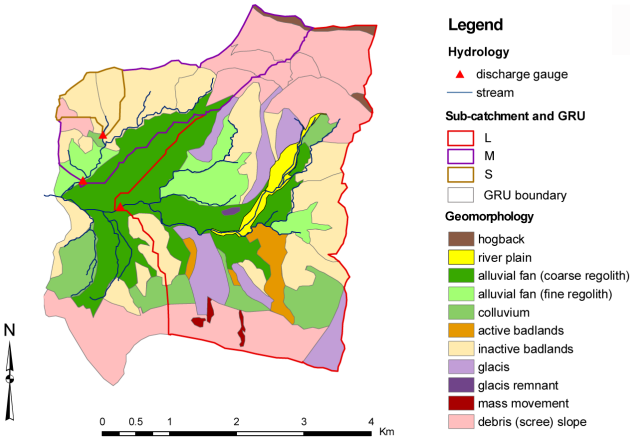

Fig. 4. Geomorphology and GRUs of the catchment.

K_S was chosen for calibration because it is a key parameter governing the mechanism of Hortonian runoff generation. Calibration of K_S was done by adjusting a single prefactor, added to K_S as a multiplier (i.e. calibration factor) for the entire domain, using a brute force calibration approach. The calibration factors were defined as a sequence of discrete values ranging from 0.1 to 500. The optimal calibration factor of K_S is the value that results in the best E, evaluated for all calibration events. To avoid the effect of outliers, we used the median.

It is preferable to use a single optimal calibration factor that is suited for all events observed in all catchments. This is to satisfy the assumption used in the parameterization of K_S to the GRUs that soil hydraulic properties of specific geomorphologic units are invariant in the catchment, and also to maintain the relative order of K_S values for the GRUs after calibration. However, physical characteristics of the S catchment are significantly different from the other catchments. More than 90 % of the S catchment area is dominated by a badlands topography and scree slopes with sparse vegetation cover, while the other two catchments are mainly characterised by alluvium or colluvium deposits with agricultural activities and forests. Including events from the S catchment would introduce a bias in the identification of the optimal calibration factor for the entire catchment. Therefore, a second optimal calibration factor was exclusively derived for the S catchment. The optimal calibration factor for L and M catchments were identified together because the physiographic characteristics are quite comparable between these catchments.

We evaluated the performance of the models using the closure relation C and C^* (both with and without calibration) with a separate set of events not used in the calibration (i.e. validation set). Performance of the closure relations was evaluated in terms of response signature (i.e. hydrograph), measured with E, and discharge quantity. Percent error in discharge volume ($e_{Q_{\mathrm{cum}}}$) is computed as

$$e_{Q_{\mathrm{cum}}} = \left| \frac{Q_{\mathrm{cum,\,sim}} - Q_{\mathrm{cum,\,obs}}}{Q_{\mathrm{cum,\,obs}}} \right| \cdot 100 \qquad (21)$$

with $Q_{\mathrm{cum,\,obs}}$ and $Q_{\mathrm{cum,\,sim}}$ (m^3) being the total observed and simulated discharge volume, respectively.

For the qualitative interpretation, the closure relation is considered as having a "good" performance with E larger than 0.4 or $e_{Q_{\mathrm{cum}}}$ smaller than 50 %; "satisfactory" with E between 0–0.4 or $e_{Q_{\mathrm{cum}}}$ between 0–50 %. The term "poor" is used to describe the simulation with E less than zero or $e_{Q_{\mathrm{cum}}}$ larger than 100 %.

3 Results

3.1 Identification of GRUs, soil properties, and catchment discharge

The catchment was classified into 11 types of major geomorphologic units, from which 59 GRUs were derived (Fig. 4, Table 2). Statistics of the measured K_S values for different types of GRU (Table 3) show large variation, which will be partly due to measurement errors. Determination of K_S using the rainfall simulation method is notably difficult due to a number of factors related to the experimental setup introducing errors in the measurements (i.e. leakage, raindrop size, rain intensity, and so on). Large variation in the measured K_S values can also be explained by the nature of K_S being variable in space. As the K_S measurements are not available for all types of GRUs and measured values will include measurement errors, it is decided to use K_S values proposed in Rawls et al. (1982) (Table 4). The K_S values provided by Rawls et al. (1982), derived from the pedo-transfer functions, are somewhat lower than those measured in our catchment. We will discuss this after presenting calibrated K_S values, which can be compared to the values observed in our catchment and those from Rawls et al. (1982).

Table 2. Characteristics of GRUs for catchments.

Catchment	N	Area (10^3 m^2)		s (m m^{-1})		L (m)	
		max	min	max	min	max	min
L	44	1140	21	0.74	0.03	1737	76
M	12	776	27	0.61	0.09	1501	196
S	3	288	53	0.38	0.18	1035	307

N: number of GRUs; s: slope (m m^{-1}); L: length (m).

More than 30 rainstorm events were observed during the study period (Table 5). Characteristics of observed rainfall events depict seasonal differences. Events in summer and autumn (i.e. July–October) were mainly observed as isolated events with a relatively high intensity (i.e. maximum intensity up to 0.1 m h^{-1} in 5 min). This intensity is far larger than the measured K_s values, which supports the claim that Hortonian runoff occurs in the study area. However, in spring and early summer, the events consisted of a set of consecutive light rainstorms, which resulted in complex hydrographs with multiple peaks that do not have a clear rising and falling limb. In this case, Hortonian runoff may have an insignificant contribution to the total event discharge. For the evaluation of the closure relations, we neglected the events with a runoff coefficient (i.e. fraction of Hortonian runoff volume to the total rainfall volume over the catchment) smaller than 0.015, which were, in total, 10 events. For these events, it is likely that the stream discharge was dominated by processes not accounted for in the closure relations, for instance direct channel precipitation (i.e. stream channels possess about 1.5 % of the catchment area). As the events were observed in the sub systems located next to each other and belong to the same catchment, inter-comparison between events in the evaluation of closure relations is possible.

Discharge used in establishing the rating curve was mostly observed during the low and moderate flow period. For half of events observed in the studied catchment, the discharge were extrapolated about 1–3 order of magnitude beyond the maximum gauged discharge. A stage-discharge relation for the S catchment is considered most reliable and valid beyond the maximum measured discharge used in constructing this relation because the cross-sectional profile and stream bed at the measurement location of water stage were stable. Discharge time series for L and M catchment were obtained with a somewhat larger degree of uncertainty compared to the S catchment. However, differences in hydrograph realizations caused by this uncertainty are not significantly large. The observed hydrograph for three catchments are considered reliable and can be used in the evaluation of closure relation performance.

3.2 Model sensitivity

The sensitivity analysis gives similar results for closure relations C and C^*. Of the parameters related to the soil, the

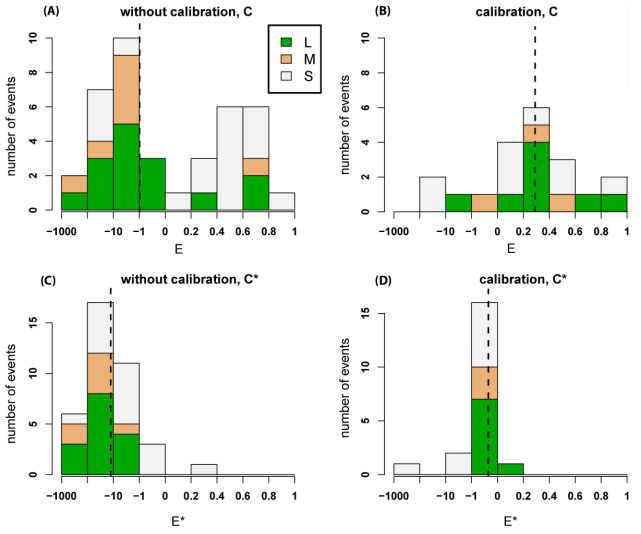

Fig. 5. Nash–Sutcliffe index (E) in the L, M and S catchment calculated for the closure relations C (top panels, **A** and **B**) and C^* (bottom panels, **C** and **D**). Left panels, without calibration; right panels, with calibration. Vertical dashed lines indicate the median of the Nash–Sutcliffe index. Note that plots on the right panel show the evaluation only with the validation events.

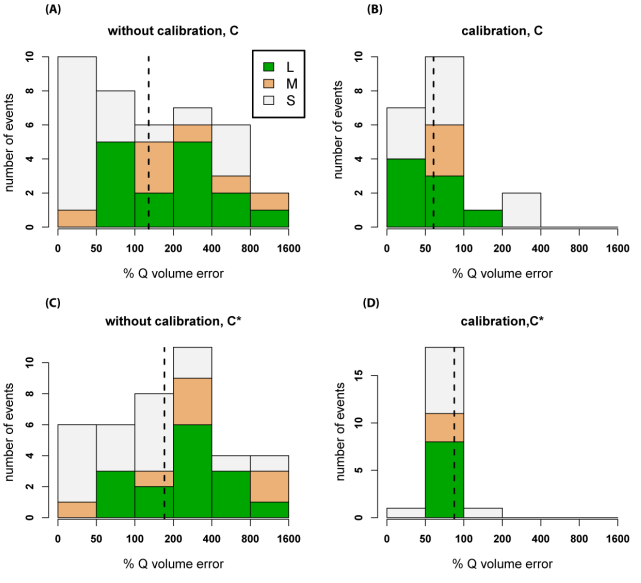

Fig. 6. Percent error in total discharge prediction ($e_{Q_{\mathrm{cum}}}$) in the L, M and S catchment calculated for the closure relations C (top panels, **A** and **B**) and C^* (bottom panels, **C** and **D**). Left panels, without calibration; right panels, with calibration. Vertical dashed lines indicate the median of the Nash–Sutcliffe index. Note that plots on the right panel show the evaluation only with the validation events.

Table 3. Comparison of saturated hydraulic conductivity (K_s; mm h^{-1}) values observed in the study area and the calibrated values used in the closure relation C and C^*.

Unit type	Field measurements					Calibrated values used in the closure relation	
	N	min	max	mean	S.D.	C	C^*
Alluvial fan (coarse regolith)	201	9	125	76	25	52	860
Alluvial fan (fine regolith)	126	15	125	64	26	28	460
colluvium	10	22	101	67	22	28	460
River plain	60	10	125	87	29	52	860

N: number of measurements; S.D.: standard deviation.

Table 4. Soil texture and corresponding soil hydraulic parameters (K_s and H_f) estimated for each type of geomorphologic unit (Rawls et al., 1982).

Geomorphologic unit	Soil/regolith type	K_s (mm h^{-1})	H_f (m)
Hogback	outcrops	0.01	-10^{-5}
River plain	sandy clay loam	4.3	−0.449
Alluvial fan (coarse regolith)	sandy clay loam	4.3	−0.449
Alluvial fan (fine regolith)	clay loam	2.3	−0.446
Colluvium	clay loam	2.3	−0.446
Active badlands	black marls	0.6	−0.714
Inactive badlands	silt clay	0.9	−0.647
Glacis	slit loam	6.8	−0.404
Glacis remnant	silt loam	6.8	−0.404
Mass movement	loamy sand	61.1	−0.142
Debris slope	loamy sand	61.1	−0.142

closure relations appear to be most sensitive to changes in K_s, both regarding discharge volume and peak discharge. The closure relations are less sensitive to the vegetation parameters (i.e. LAI and $S_{I,\,leaf}$). The time to the peak discharge is almost unaffected by changes in both soil and vegetation parameters. The benchmark closure relation C^* is slightly more sensitive to the change of model parameters compared to C.

The Manning's coefficient n is the most sensitive parameter in terms of timing in discharge responses. Increasing n to 0.05 results in a delay of the peak discharge up to 25 min for both closure relations, compared to the simulations from the base runs (i.e. $n = 0.03$). This delay increases with the catchment size. Changing the Manning's n has no effect on the total discharge volume.

The model is found to be sensitive to changes in the initial soil moisture content, particularly when the soil wetness condition is close to saturation. Thus, estimation of soil moisture might have an effect on our model results. However, differences in soil moisture estimated by different evapotranspiration models are quite small, particularly in the wet period. Differences become larger when the soil dries out – about 20–25 % in the dry period (not shown). However, in this condition, the model appears to be less sensitive to the change in moisture content. Considering these findings, it can be stated that the choice of evapotranspiration models used for estimation of initial moisture content does not have remarkable effects on our evaluation of the closure relations.

3.3 Simulation of discharge without calibration

The closure relation C shows a "good" performance in simulating the shape of hydrograph (i.e. $E > 0.4$) for more than 30 % of the events observed in the three catchments (Fig. 5a). Performance of closure relation C is particularly high for events in the S catchment, where predictions of the hydrograph shape are "good" for almost 60 % of the events observed in this catchment. However, it is shown that the hydrograph magnitude is largely overestimated for a number of events, resulting in extremely low (negative) E values (Table 8). Regarding the relative performance, the closure relation C is capable of simulating discharge responses better than the benchmark closure relation C^* (Fig. 5a, c and Table 8). The closure relation C^* appears to have almost no predictive capability for the hydrograph responses as E values are far below zero for most events (Fig. 5c, Table 8).

Table 5. Characteristics of the rainstorm events selected for evaluation of closure relations.

Catchment	N	R_{avg} (mm h^{-1})				T (h)				Runoff coefficient (–)			
		min	med	max	S.D.	min	med	max	S.D.	min	med	max	S.D.
L	15	2.0	4.5	34.6	10.4	0.4	4.3	27.9	7.9	0.02	0.04	0.11	0.03
M	7	4.0	5.1	8.0	1.8	3.6	5.5	9.4	8.0	0.017	0.04	0.13	0.04
S	17	2.0	4.1	29.3	7.7	0.4	3.9	23.5	6.9	0.015	0.08	0.3	0.09

R_{avg}: average rainfall intensity (mm h^{-1}); T: event duration (h); N: number of events; med: median; S.D.: standard deviation.

Table 6. Sensitivity of the model results with the closure relation C. Values are averaged over all events ($n = 13$).

Catch-ment	Model results	% Change in parameter value	Average changes in the model results					
			K_s	H_f	θ	LAI	$S_{I,leaf}$	n^*
L	Q_{cum}	−25	13 %	7 %	−9 %	2.54 %	2.57 %	−0.01 %
		25	−9 %	−5 %	5 %	−2.45 %	−2.45 %	0 %
	Q_{max}	−25	13 %	10 %	−11 %	3.26 %	3.57 %	1.15 %
		25	−9 %	−6 %	4 %	−2.67 %	−2.48 %	−3.27 %
	t_p	−25	0 h	0 h	0.01 h	−0.01 h	0 h	−0.17 h
		25	0.01 h	−0.01 h	0.01 h	0 h	0.01 h	0.38 h
M	Q_{cum}	−25	14 %	6 %	−6 %	2 %	2 %	0 %
		25	−9 %	−4 %	8 %	−1 %	−1 %	0 %
	Q_{max}	−25	15 %	9 %	−11 %	2 %	3 %	0 %
		25	−10 %	−6 %	5 %	−1 %	−1 %	−1 %
	t_p	−25	−0.07 h	0.01 h	0.05 h	0 h	0 h	−0.12 h
		25	0.01 h	0.02 h	−0.06 h	0 h	0 h	0.2 h
S	Q_{cum}	−25	18 %	12 %	−15 %	1 %	1 %	0 %
		25	−10 %	−7 %	9 %	−1 %	−1 %	0 %
	Q_{max}	−25	18 %	14 %	−22 %	1 %	1 %	0 %
		25	−11 %	−8 %	7 %	−1 %	−1 %	−2 %
	t_p	−25	−0.01 h	−0.02 h	0 h	0 h	0 h	−0.04 h
		25	0 h	0 h	0 h	0 h	0 h	0.06 h

Q_{cum}: total discharge volume; Q_{max}: peak discharge; t_p: time at the peak discharge; K_s: saturated hydraulic conductivity; H_f: matric suction at the wetting front; θ: initial moisture content; LAI: leaf area index; $S_{I,leaf}$: maximum interception capacity per LAI; n: Manning's coefficient. Note that changes regarding t_p are expressed as the averaged absolute time difference from the standard runs (h). * Values of Manning's n used in the sensitivity analysis are 0.02 and 0.05, instead of ±25 %.

Hydrographs of an individual event (Fig. 7a, c, and e) simulated by the closure relation C^* exhibit an almost instantaneous discharge response to rainfall, resulting in hydrographs that closely follow rainfall intensity and severely overestimate runoff response. The closure relation C, on the other hand, produces a smoother hydrograph with more delay in runoff responses relative to the rainfall. Although the magnitude of discharge is overestimated when using the closure relation C, the shape of the modelled hydrograph is comparable to the observed hydrograph. The discrepancy between observed and modelled hydrographs is smallest for the S catchment. To provide a more comprehensive evaluation of the closure relation performance on an event basis, additional plots of observed and simulated discharge for a number of selected events are given in an Appendix A.

The relative performance of C and C^* regarding errors in total discharge volume (Fig. 6a and c) is similar to the results observed when considering E. The closure relation C gives a more accurate prediction of total discharge volume compared to C^*. The closure relation C has a "good" performance for 25 % of the total events, while this number decreases to 15 % for the benchmark closure relation C^*. Both closure relations C and C^* give the smallest prediction errors in the total discharge volume in the S catchment. However, the absolute performance in terms of errors in total discharge volume is rather low for both $C$and C^*. Discharge volume is, in general, largely overestimated for most of the events, except for catchment S where discharge volume is underestimated for the high-intensity rainfall events. Errors in total discharge volume do not differ considerably between closure relation C and C^* (Table 8).

Table 7. Sensitivity of the model results with the closure relation C^*. Values are averaged over all events ($n = 13$).

Catchment	Model results	% Change in parameter value	Average changes in the model results					
			K_s	H_f	θ	LAI	$S_{I,leaf}$	$n*$
L	Q_{cum}	−25	15 %	10 %	−11 %	3 %	3 %	0 %
		25	−10 %	−6 %	4 %	−3 %	−3 %	0 %
	Q_{max}	−25	16 %	11 %	−13 %	7 %	7 %	5 %
		25	−10 %	−8 %	4 %	−3 %	−3 %	−10 %
	t_p	−25	0.01 h	−0.3 h	0.03 h	0.03 h	0.04 h	−0.46 h
		25	0.03 h	0.02 h	−0.04 h	0.05 h	0.04 h	0.42 h
M	Q_{cum}	−25	15 %	9 %	−10 %	2 %	2 %	0 %
		25	−10 %	−6 %	8 %	−1 %	−1 %	0 %
	Q_{max}	−25	21 %	15 %	−10 %	2 %	3 %	6 %
		25	−13 %	−10 %	8 %	−1 %	−1 %	−4 %
	t_p	−25	0.01 h	0.02 h	0.08 h	0 h	0 h	−0.11 h
		25	0 h	0 h	−0.1 h	−0.01 h	0.01 h	0.1 h
S	Q_{cum}	−25	22 %	17 %	−21 %	1 %	1 %	0 %
		25	−11 %	−8 %	9 %	−1 %	−1 %	0 %
	Q_{max}	−25	32 %	24 %	−26 %	0 %	0 %	−2 %
		25	−10 %	−8 %	8 %	0 %	−1 %	−4 %
	t_p	−25	0.04 h	0.04 h	0.02 h	0 h	0 h	−0.04 h
		25	0 h	0 h	0.02 h	0 h	0 h	0.02 h

Q_{cum}: total discharge volume; Q_{max}: peak discharge; t_p: time at the peak discharge; K_s: saturated hydraulic conductivity; H_f: matric suction at the wetting front; θ: initial moisture content; LAI: leaf area index; $S_{I,leaf}$: maximum interception capacity per LAI; n: Manning's coefficient. Note that changes regarding t_p are expressed as the averaged absolute time difference from the standard runs (h). * Values of Manning's n used in the sensitivity analysis are 0.02 and 0.05, instead of ±25 %.

3.4 Simulation of discharge with calibration

3.4.1 Derivation of the calibration factors

Characteristics of the calibration events (Table 9), except for event duration, are not statistically different from the events used for validation of the closure relations (statistical tests on mean and variance differences not shown). Also, the predictive performance of closure relations for these two event groups is quite comparable (Table 10). It can be asserted that the events used for calibration have similar characteristics to the events for validation. The optimal calibration factors can be derived without a remarkable bias caused by differences between two groups of events.

Figure 8a and b show the values of the Nash–Sutcliffe coefficient (E) for different calibration factors. Although we aim at deriving optimal calibration factors based on E, effects of the calibration factor on the percent error in discharge volume, $e_{Q_{cum}}$, were also investigated (Fig. 8c and d). This is to provide an insight into the capability of closure relations to predict the discharge volume. The optimal calibration factor for each catchment can be visually identified from the highest point in the response line of the Nash–Sutcliffe coefficient; and the lowest point in the response line of $e_{Q_{cum}}$.

For the closure relation C, the response line for the Nash–Sutcliffe coefficient clearly shows a single optimum. According to Fig. 8a, the optimal calibration factor of 12 found for the L and M catchment is larger than the value obtained for the S catchment, which was 5. For the S catchment, a calibration factor of 1 results in a similar value for E as found when using a calibration factor of 5. This supports the findings in Sect. 3.3 that the closure relation C can be used to simulate discharge in this catchment without calibration (i.e. calibration factor = 1). The calibration factors resulting in the lowest median of E are not very different from those resulting in the lowest median of $e_{Q_{cum}}$ (Fig. 8a and c), allowing the use of a single calibration factor that performs well regarding both E and $e_{Q_{cum}}$.

It is difficult to identify a single optimal calibration factor for the closure relation C^*. The median of E gradually increases with an increase in the calibration factor, but never exceeds zero (Fig. 8b). The best median of E was found at an extremely high calibration factor. Here, we selected the highest calibration factor, 200, as an optimum for the L and M catchment, while a calibration factor of 20 was chosen for the S catchment. Contrary to the response line for the Nash–Sutcliffe coefficient, the line for $e_{Q_{cum}}$ shows a clear optimum (Fig. 8d) for C^*. The optimal calibration factors for closure relation C^* for $e_{Q_{cum}}$ are similar to the values obtained for closure relation C (Fig. 8c and d).

In principle, calibration of the closure relation for the correct hydrograph shape should already be sufficient because it

Table 8. Performance of C and C^* without calibration.

Catchment	N	Closure relation	E				$e_{Q_{\text{cum}}}$			
			min	med	max	S.D.	min	med	max	S.D.
L	15	C	−115.5	−2.6	0.78	35.6	54.2	205.6	879.9	233.9
		C^*	−983.6	−40.3	−3.6	264.5	50.8	277.0	1271.0	311.8
M	7	C	−292.0	−8.2	0.64	107.2	32.2	197.6	1462.0	506.3
		C^*	−875.2	−23.8	−3.2	327.6	35.0	238.2	1565.0	545.4
S	17	C	−84.5	0.5	0.84	25.6	12.2	36.9	781.7	244.1
		C^*	−2573.0	−6.9	0.24	619.9	10.0	101.0	1378.0	359.7
Total	39	C	−292.0	−0.9	0.84	52.6	12.2	136.0	1462.0	306.9
		C^*	−2573.0	−19.2	0.24	452.7	10.0	176.8	1565.0	378.7

N: number of events; E: Nash–Sutcliffe index; $e_{Q_{\text{cum}}}$: percent error in total discharge volume; med, median; S.D.: standard deviation.

Table 9. Statistics of the calibration and validation events.

Catchment	Event type	N	R_{avg} (mm h^{-1})				T (h)				Runoff coefficient (–)			
			min	med	max	S.D.	min	med	max	S.D.	min	med	max	S.D.
L	calibration	7	2.0	3.2	34.6	11.9	0.4	4.5	8. 7	2.9	0.02	0.03	0.05	0.01
	validation	8	2.0	5.5	30.4	9.7	0.7	3.5	27.9	10.5	0.02	0.05	0.11	0.03
M	calibration	4	4.2	4.7	7.4	1.5	3.6	5.1	7.3	1.6	0.02	0.04	0.05	0.16
	validation	3	4.0	7.3	8.0	2.2	3.8	11.4	26	11.3	0.03	0.08	0.13	0.52
S	calibration	8	2.4	3.8	29.3	9.9	0.4	4.3	8.9	3.0	0.04	0.07	0.14	0.04
	validation	9	2.0	4.2	19.4	5.3	0.8	3.8	23.5	8.9	0.02	0.13	0.3	0.11

R_{avg}: average rainfall intensity (m h^{-1}); T: event duration (h); N: numbers of events; med, median; S.D.: standard deviation.

will also simultaneously result in the simulations with correct discharge volume. Therefore, the calibration factor found for the optimal E is chosen for validation of the closure relations.

3.4.2 Validation results

The performance of the closure relation C is considerably improved after calibration, as can be seen in Fig. 5, right panels. The calibrated closure relation C has "good" and "satisfactory" performance in predicting the hydrograph shape (i.e. according to E) for 30 and 50 % of the validation events, respectively (Fig. 5b). The best E obtained after calibration is 0.8 with a median of 0.3, which is slightly worse than what is found for the calibration events (i.e. 0.4). The results also show that, after calibration, C is capable of reproducing the observed total discharge using the calibration factor optimised regarding E (Fig. 6b). This result was expected because the optimal calibration factors that result in the lowest median of $e_{Q_{\text{cum}}}$ are quite similar to those found for E (Fig. 8a and c). Predictive capability of the closure relation C after calibration is somehow exacerbated for a number of events observed in the S catchment, as shown by a lower median of E compared to the case of without calibration (Table 11).

Contrary to the calibrated closure relation C, the benchmark closure relation C^* has low performance in simulating the hydrograph shape after calibration. Almost 80 % of the validation events have an E between −1 and 0 (Fig. 5d). The median E calculated for the validation events is still below zero for all catchments (Table 11). Although the magnitude of hydrograph and peak discharge can be reduced as comparable to the observations, the shape of simulated hydrographs represents a too instantaneous response to rainfall (Fig. 7b, d, and f). It is obvious that calibration of C^* is not sufficient to retrieve good results for E. This is also indicated by the small changes in hydrograph shape when changing the calibration factor (Fig. 9a, c, e), reflecting the incapability of the closure relation C^* in representing Hortonian runoff at the scale of a GRU even with an ad hoc parameterization. Unlike C, the calibrated C^* gives unsatisfactory predictions of the discharge volume with the calibration factor optimised on E. Figure 6d indicates that only one validation event has "good" prediction of total discharge. However, when C^* is calibrated on discharge volume, validation results for cumulative discharge are considerably better (Fig. 9b, d, and f). We can conclude here that it is only feasible to calibrate the benchmark closure relation C^* to have a correct discharge volume, but not for a correct shape of the hydrograph.

Table 10. Performance of non-calibrated closure relations evaluated for calibration and validation events.

Catchment	Event types	E				$e_{Q_{cum}}$			
		C		C^*		C		C^*	
		med	S.D.	med	S.D.	med	S.D.	med	S.D.
L	calibration	−6.5	41.4	−72.2	172.0	256.4	186.2	277.0	200.5
	validation	−0.9	30.6	−25.7	338. 5	111.8	276.3	237.3	399.6
M	calibration	−23.1	138.3	−193.5	402.4	438.4	608.7	524.5	658.4
	validation	−3.7	4.6	−19.2	14.4	144.0	99.4	229.4	116.4
S	calibration	0.35	20.8	−12.4	85.6	83.3	221.0	138.2	244.4
	validation	0.52	30.1	−2.9	854.3	29.9	276.5	64.1	441.2

N: number of events; med, median; S.D.: standard deviation; E: Nash–Sutcliffe index; $e_{Q_{cum}}$: percent error in total discharge volume.

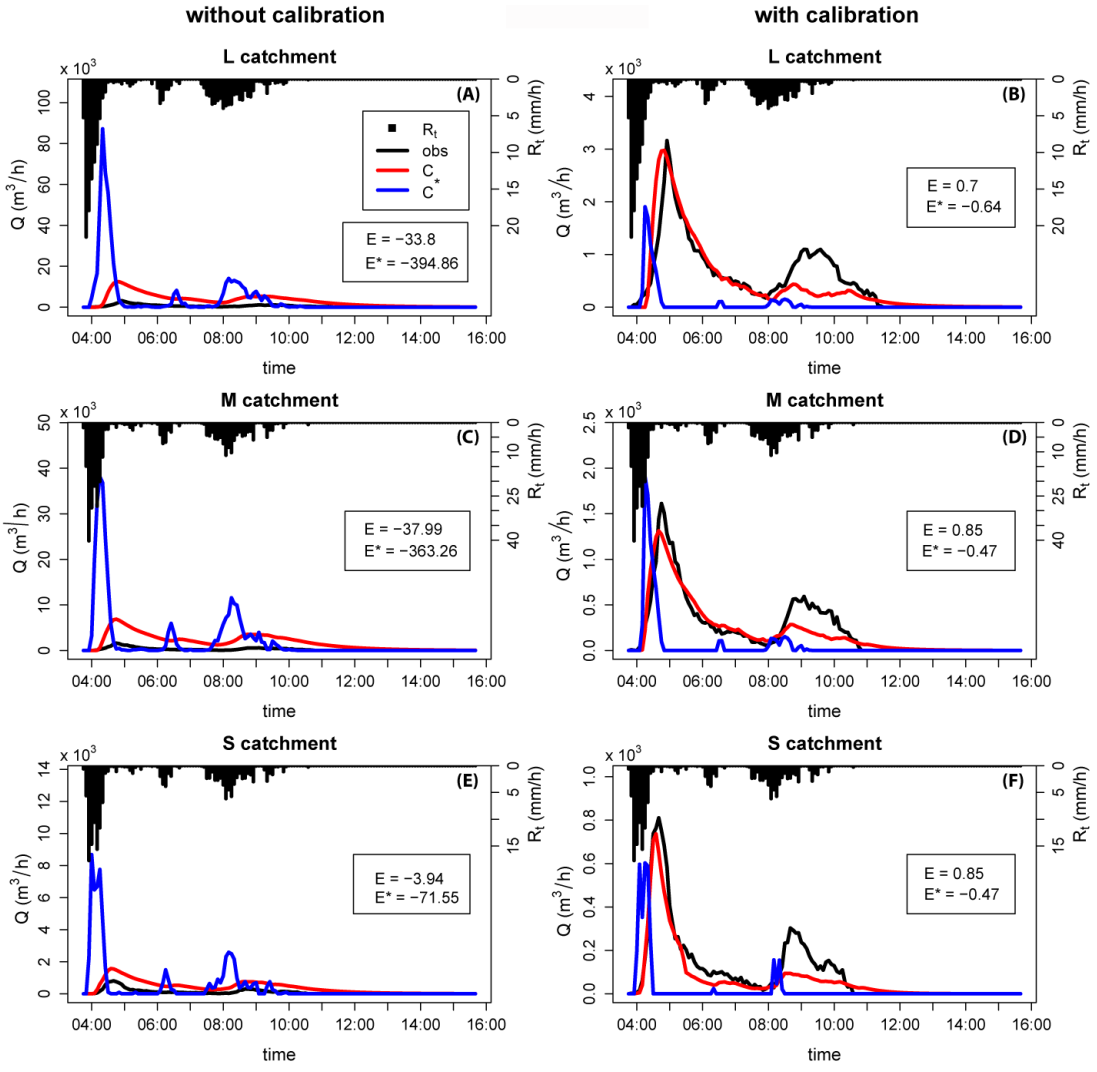

Fig. 7. Hydrographs (Q, $m^3\,h^{-1}$) modelled using the closure relation C (red) and C^* (blue) and observed (obs, black), for an event on 17 June 2010. Rainfall intensity (R_t, $mm\,h^{-1}$) is shown on the secondary axis. E and E^* are the Nash–Sutcliffe indexes for the closure relation C and C^*, respectively. Left **(A, C, E)** panels, without calibration; right panels **(B, D, F)**, with calibration.

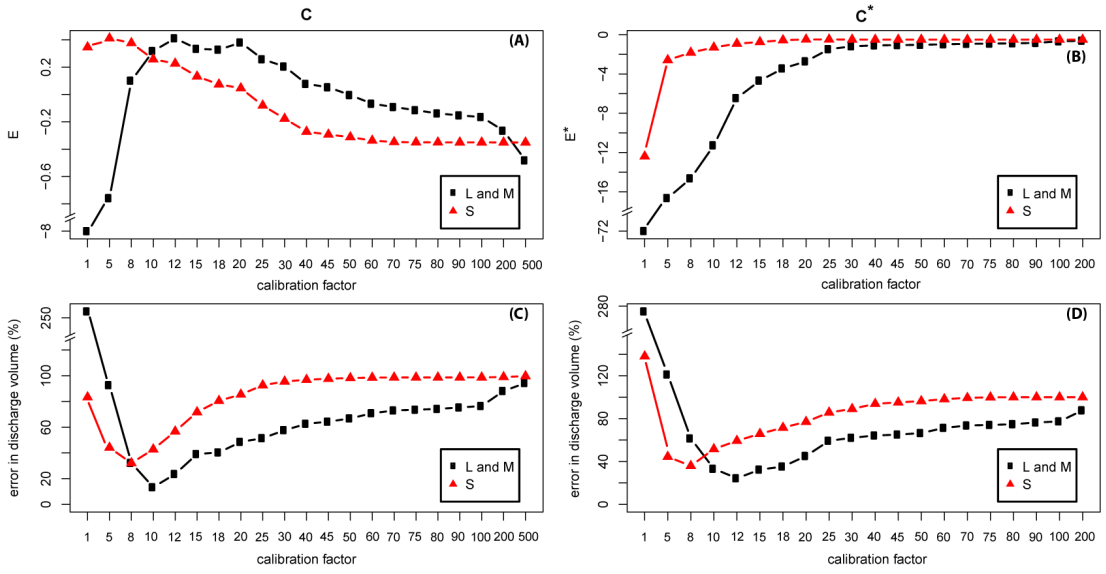

Fig. 8. Median of the Nash–Sutcliffe index, E (**A** and **B**), and discharge volume error as a percentage (**C** and **D**) calculated from events used for calibration (y axis) as a result of different calibration factors (x axis) for L and M catchments together (black line, rectangular dots), and S catchment (red lines, triangle dots) for the closure relation C and C^*.

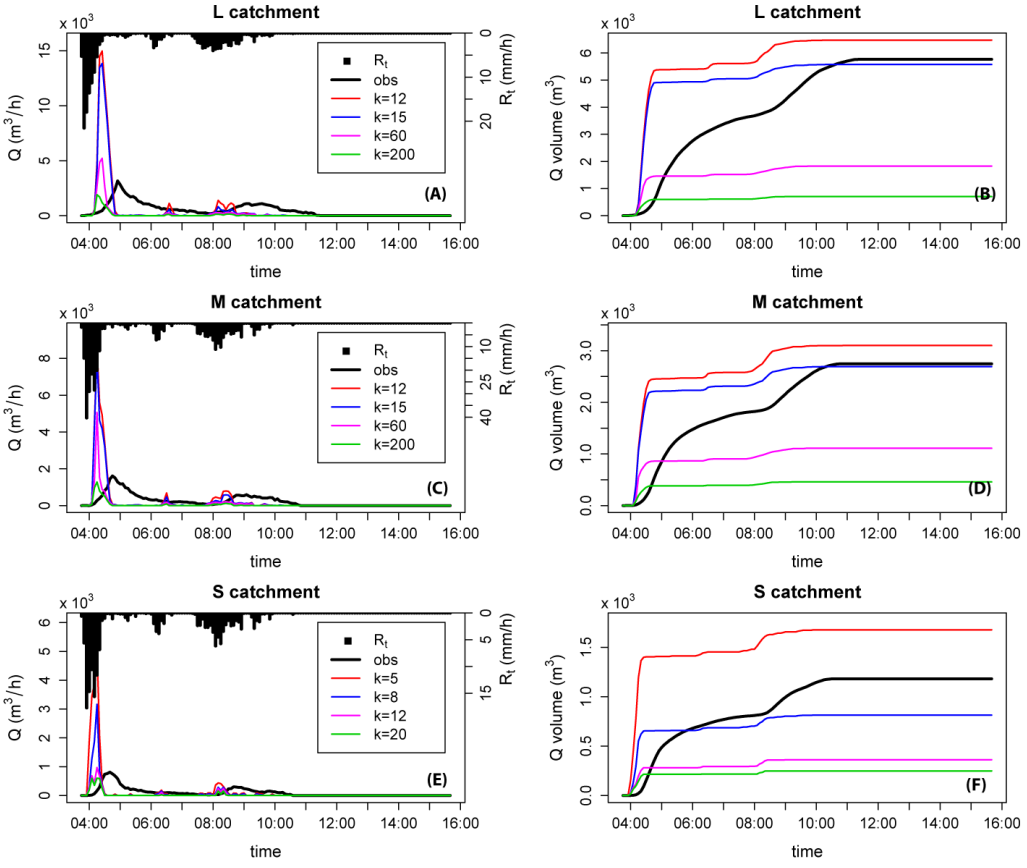

Fig. 9. Hydrographs ($m^3\,h^{-1}$, left panel: **A, C, E**) and the corresponding cumulative discharge volume (m^3, right panel: **B, D, F**) from individual catchments simulated using the closure relation C^* with different calibration factors, k, for the event observed on 17 June 2010. Rainfall intensity (R_t, $mm\,h^{-1}$) is plotted on the secondary axis.

Table 11. Performance of C and C^* after calibration.

Catchment	N	Closure relations	E				$e_{Q_{\text{cum}}}$			
			min	med	max	S.D.	min	med	max	S.D.
L	8	C	−1.2	0.32	0.81	0.6	14.3	48.2	132.0	36.7
		C^*	−0.6	−0.4	0.07	0.2	74.3	84.6	96.4	8.5
M	3	C	−0.7	0.36	0.44	0.6	55.3	63.4	68.5	6.7
		C^*	−0.5	−0.36	−0.3	0.2	72.9	92.6	95.8	12.4
S	9	C	−16.3	0.13	0.86	6.5	11.8	72.9	308.2	103.9
		C^*	−165.6	−0.3	−0.03	55	49.6	88.2	191.7	41.5
total	20	C	−16.3	0.3	0.86	4.5	11.8	60. 7	308.2	72.3
		C^*	−165.6	−0.35	0.07	36.9	49.6	87.5	191.7	27.8

N: number of events; E: Nash–Sutcliffe index; $e_{Q_{\text{cum}}}$: percent error in total discharge volume, med, median; S.D.: standard deviation.

Performance of the calibrated closure relation C is considered as "poor" in terms of E and $e_{Q_{\text{cum}}}$ for events with a runoff coefficient smaller than 0.02. For these events, the hydrograph peak and total discharge volume are considerably overestimated. The calibrated closure relation C exhibits the highest performance for events with a runoff coefficient between 0.05–0.1, beyond which the performance of calibrated C gradually decreases with increasing runoff coefficient (Fig. 10a and b). Relations between $e_{Q_{\text{cum}}}$ and the runoff coefficient (Fig. 10b) show a pattern comparable to those found for E; the smallest discharge volume errors are found at intermediate values of the runoff coefficient. For events with a high runoff coefficient, the calibrated closure relation C tends to underestimate the amount of discharge. In some extreme cases, the discharge is considerably underestimated or almost not generated, resulting in a value of $e_{Q_{\text{cum}}}$ that almost reaches 100 % (Fig. 10b). With the use of calibration factor optimised for best median E in all calibration events, performance of the calibrated closure relation C is optimal for events with a moderate runoff coefficient. The calibrated closure relation C^* does not exhibit a trend in performance runoff coefficient because the discharge was poorly simulated for most events.

4 Discussion and conclusion

This study aimed at evaluating, at the catchment scale, the performance of a previously developed closure relation for GRU-scale Hortonian runoff. This closure relation, C, incorporates scaling parameters to account for sub-GRU process heterogeneity. These scaling parameters can be obtained as a function of rainstorm characteristics and measurable GRU properties, using relations derived from an extensive synthetic data set given in Vannametee et al. (2012). The closure relation was incorporated in a rainfall–runoff model, which was applied to a first-order catchment in the French Alps. The catchment was divided into 59 GRUs corresponding to dominant geomorphological features. Performance of the closure relation C was evaluated on an event basis under two circumstances that are often encountered in the hydrological modelling – a gauged (i.e. non-calibrate) and an ungauged (i.e. calibrate) situation. To assess the relative performance of our closure relation, results were compared to results from a benchmark closure relation C^* that does not incorporate scaling parameters.

The results show that the closure relation C clearly outperforms the benchmark closure relation C^*, with respect to the Nash–Sutcliffe coefficient and error in total discharge volume for most events. The closure relation C is capable of reproducing the hydrograph shape for our study catchment, even without calibration. Shape and timing of responses of the simulated hydrographs by the non-calibrated C are in accordance with the observed discharge; however, the response magnitude and discharge volumes are overestimated for a number of events. Contrary to our closure relation C, it is impossible to obtain accurate discharge responses using the closure relation C^* that does not correct for sub-GRU processes. Discharge responses reproduced by C^* are too dependent on the temporal characteristics of storm intensities. Furthermore, the discharge volume is considerably overestimated.

Calibration of K_s in the closure relation C simultaneously improves the shape of the hydrograph and total discharge volume, resulting in K_s values that are 5–12 times higher than the original (uncalibrated) values. The calibrated K_s values in the closure relation C are somewhat smaller than those measured in the study area, but fall within the range of observed K_s (Table 3). The measured K_s values exhibit large variation, which is caused by measurement errors and large variation of K_s over short distances (Karssenberg, 2006). The calibrated K_s values also lie within the range of K_s values observed at the plot scale in other studies (e.g. Robichaud, 2000; Harden and Scruggs, 2003; Stone et al., 2008; Langhans et al., 2011; Van den Putte et al., 2012). According to this result, it can be asserted that, as the scale effects are isolated and explicitly accounted for by the scaling parameters in the closure relation C, the calibrated K_s values represent

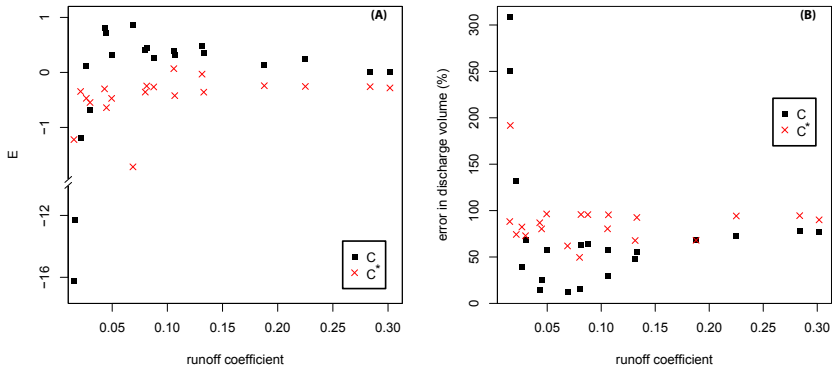

Fig. 10. Performance of the calibrated closure relation C and C^* versus the runoff coefficient of events. **(A)** Nash–Sutcliffe index; **(B)** percent error in discharge volume.

local (plot) scale values. This finding implies that our closure relation C may be used for the discharge prediction even without calibration, particularly when sufficient empirical information is available on local (plot) scale values of K_s. Unlike C, the benchmark closure relation C^* is incapable of reproducing observed hydrographs, even after calibration. As the benchmark closure relation C^* neglects scaling effects, process description is grossly simplified as analogous to the runoff-generation processes at a plot scale; runoff was modelled as an infiltration-excess flux that is instantaneously discharged from the GRUs without delay, resulting in hydrographs with a too steep rising and falling limb compared to the observed hydrographs. Also, calibrated K_s values for the benchmark closure relation C^* are considerably higher than those measured in the study area (Table 3) or reported in other studies. The calibrated K_s used in the benchmark closure relation C^* appears to have a limited physical meaning. However, after calibration, the benchmark closure relation C^* is capable of providing reliable estimates of discharge volume, albeit with hydrograph shape different from those observed. It can be stated here, as a side remark, that calibration of K_s does not significantly compensate for the uncertainty in the choice of parameters used in the model forcing or routing components because the model is by far most sensitive to the changes in K_s and infiltration parameters compared to the changes in vegetation and channel parameters.

The capability of the closure relation C to reproduce discharge using local scale K_s values as input, can be attributed to the use of scaling parameters to account for the effects of the GRU's geometry (e.g. length, slope gradient, and connectivity in flow pattern) and sub-GRU processes (e.g. post-event infiltration, GRU storage) on the response characteristics at the GRU scale (i.e. lag of responses, attenuation of responses, and so on). Errors in the discharge magnitude of the non-calibrated runs are mainly caused by the uncertainty in the local-scale infiltration parameters (i.e. K_s and H_f) and boundary conditions. It is shown that, in the S catchment, where the infiltration parameters can be estimated with less uncertainty (i.e. GRUs have small infiltration capacity), discharge simulated using the uncalibrated C is already quite accurate for a large number of events. For the benchmark closure relation C^*, calibration does not remarkably improve the discharge prediction, which is a strong indication that C^* does not properly capture the processes in the GRUs. It might be possible to improve the performance of the benchmark closure relation C^* by calibrating a larger number of parameters. Even if this were possible, the performance of the benchmark closure relation would largely rely on calibration, without the benefit of using observable watershed characteristics as in our closure relation C. The result would be a model with a weaker physical basis compared to our closure relation, because the issue of model structural inadequacy (Gupta et al., 2012) is not resolved.

The absolute performance of C might be considered not very impressive in some events. However, this is still acceptable for several reasons. In this study, we do not present the model development at an operational stage, but merely evaluate the performance of C and a merit of incorporating the scaling component in the closure relation. Evaluation was done on a relative basis by comparing the Nash–Sutcliffe coefficient E obtained from the simulations by C and C^*. As it is not our aim to maximise E, some model components are kept simple (i.e. interception and routing scheme) and calibration is restricted to the most sensitive parameter, using simple calibration approach. Apart from this, it is also notably difficult to perform event-based hydrograph prediction in a small catchment, as the errors in boundary conditions and model parameters are hardly averaged out. Other studies in a small catchment show relatively low E, as comparable to those of our studies (e.g. Meng et al., 2008). Nevertheless, we would like to note that the closure relation C yields the simulation results with quite high E for a number of events (i.e. E is large up to 0.8).

It can be argued that C^* might not be an interesting benchmark because the process description used in C^* is somewhat too oversimplified; thus the poor simulation results from C^* can be expected. The benchmark closure relation C^* essentially neglects the runoff-travel time within GRUs to

the stream network. However, this assumption is commonly made in many large-scale hydrological models, in which the closure relations can be applied. In such models, delay in runoff generated at hillslopes or the sub-grid sections is neglected or combined with the delay in the main channels in a grid cell or sub-catchment (e.g. Yu, 2000). To deal with this argument, we have somewhat improved the benchmark closure relation C^* by incorporating a component to account for the runoff-travel time within GRUs. The delay of GRU-generated runoff to the stream network is estimated using the Manning's equation (Chow et al., 1988), and assumed invariant for all GRUs as to avoid imposing the scaling element in the simulation. With the improved benchmark closure relation C^*, the simulated hydrographs at the catchment scale show a lag response, but the shape still remains incorrect (i.e. too instantaneous to the rainfall characteristics). Calibration of the improved C^* also results in an extremely high K_s, similar to those of the original C^* (results not shown). It can be concluded that performance of C^* is not significantly improved even the delay in runoff generated from GRUs is considered. This finding strengthens the fact that the process description used in C^* is not appropriate due to the lack of a scaling component.

The closure relation C exhibits the largest predictive performance for events with a moderate runoff coefficient. Predictive capacity of the non-calibrated closure relation C decreases for events with a low runoff coefficient. For these events, the hydrograph magnitude and discharge volumes are grossly overestimated. This may have various causes. One is that the closure relation C does not take into account spatial heterogeneity of the GRU properties and its effects on runoff generation. Spatial variability of infiltration parameters becomes more important in the runoff generation for low-intensity events. A deterministic process conceptualization using uniform infiltration parameters is apparently not sufficient to capture the stochastic behaviour of infiltration and runoff generation processes (Corradini et al., 1998; Karssenberg, 2006). Another limitation of our closure relation is related to the limited information on the value of scaling parameters for low intensity rainstorms, which were under-represented in the synthetic database (Vannametee et al., 2012) used to derive scaling parameters. Finally, additional errors in hydrograph estimation may occur due to errors in model inputs or structural errors in modelling framework in which the closure relation is used. In this study, we neglected seasonal dynamics of the vegetation characteristics, which might affect interception and the amount of net rain. However, this effect is not expected to be significant because the model is almost not sensitive to changes in the vegetation parameters. Overestimation of the event discharge can be also partly attributed to the assumption that no water loss occurs in the streams. Even though the amount of in-stream loss is most likely relatively small compared to the discharge generated at the catchment scale, neglecting the in-stream loss may result in an overestimation of the discharge for storm events with a small runoff coefficient. For these events, discharge is mostly generated from upstream GRUs (i.e. hogback, debris slope, and badlands) due to a smaller infiltration capacity compared to the downstream GRUs (i.e. colluvium and alluvial fan). Discharge generated at upstream GRUs is likely to be lost to deeper groundwater from the channels before it reaches the outlets.

The results from this study demonstrate the possibility of applying the closure relation C for discharge simulation in the real-world catchments. Based on these results, it can be concluded that the framework proposed by Vannametee et al. (2012) is promising and should be further investigated as an alternative blueprint in the identification of closure relations. Following this approach, closure relations for different hydrological compartments can be developed, providing a basis for lumped modelling framework under the HRU or REW concept. This approach is particularly useful because it does not entirely depend on field observations that might be costly or difficult to obtain. The closure relations can be deduced using an artificial data set, generated by a distributed high-resolution model, as a surrogate of real-world data. Future research along the line of this paper could focus on the improvement of the relations between scaling parameters in the closure relations and observable parameters for a wide range of conditions. This can be done by recalculating and extending the database to include more observable watershed characteristics in the estimation of scaling parameters and focus more on light rainstorms. Also, the level of physics used in the physically base high-resolution model for identifying the relations between scaling parameters and observables could be further improved. More importantly, other runoff generating mechanisms at the catchment scale; such as, saturated overland flow, including groundwater flow and variably saturated areas could also be considered in the modelling framework. The closure relations for these hydrological components can be developed following the hillslope-storage Boussinesq approach (Troch, 2003). Due to the fast progress in computing technology, limitations related to the available computational resources and run time will no longer be an obstacle for the aforementioned tasks. Advantages and trade-offs in using the closure relation C (either the current or improved versions) in comparison to a fully distributed hydrological model should also be investigated for catchments with different sizes; this should be done in a systematic way by looking at the simulation run time, computational costs, model efficiency, and calibration efforts.

Appendix A

Additional comparison plots between the observed and simulated discharge from the closure relation C and C^*

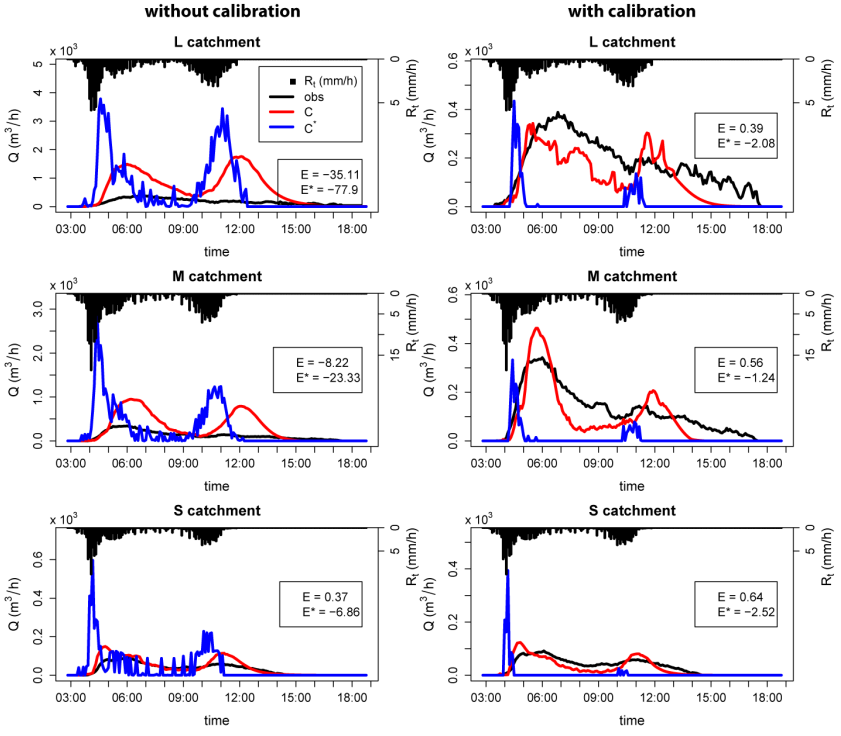

Fig. A1. Hydrographs (Q, $\mathrm{m^3\,h^{-1}}$) modelled using the closure relation C (red) and C^* (blue), compared with the observed discharge (obs, black), for an event on 1 April 2010. Rainfall intensity (R_t, $\mathrm{mm\,h^{-1}}$) is shown on the secondary axis. E and E^* are the Nash–Sutcliffe indexes for the closure relation C and C^*, respectively. Left panels, without calibration; right panels, with calibration.

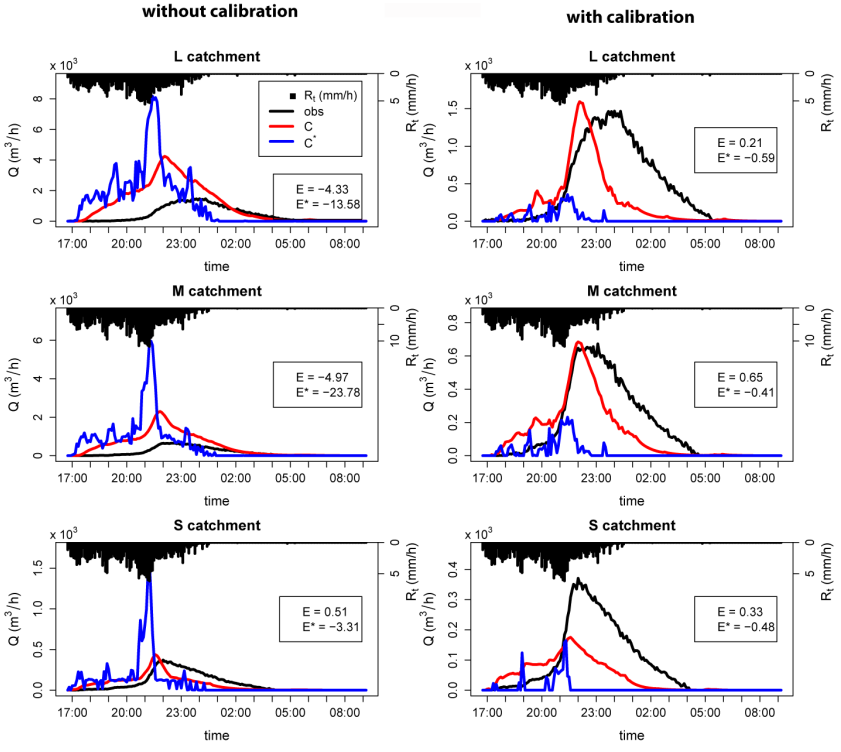

Fig. A2. Same as in Fig. A1, for an event on 7 April 2010.

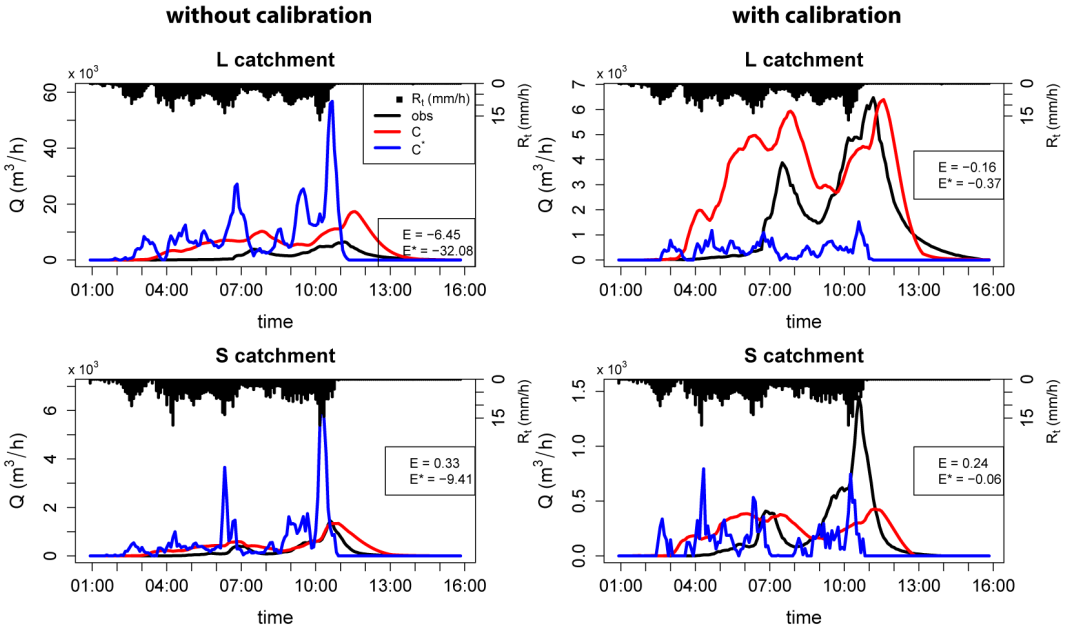

Fig. A3. Same as in Fig. A1, for an event on 7 September 2010. Note that observed discharge in the M catchment is not available for this event.

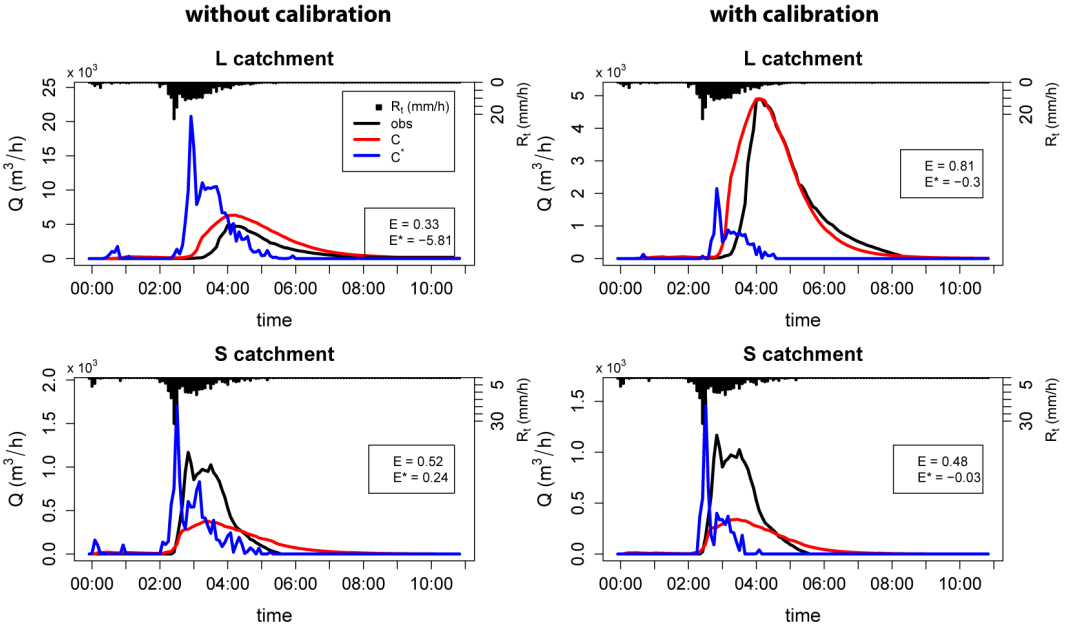

Fig. A4. Same as in Fig. A1, for an event on 8 September 2010. Note that observed discharge in the M catchment is not available for this event.

Acknowledgements. This research was funded by the Anadamahidol Foundation, under the royal patronage of the King of Thailand. The authors would like to thank M. de Jonge, L. Sapkul, C. Inchaisri, and students from the Faulty of Geosciences, Utrecht university who helped us with field data collection.

Edited by: C. Harman

References

Adhikari, R. N., Rama Mohan Rao, M. S., and Husenappa, V.: Rainfall simulator studies for the effect of soil and water conservation measures on runoff and soil loss, Indian J. Agric. Res., 37, 157–168, 2003.

Ahrens, B.: Distance in spatial interpolation of daily rain gauge data, Hydrol. Earth Syst. Sci., 10, 197–208, doi:10.5194/hess-10-197-2006, 2006.

Betrie, G. D., Mohamed, Y. A., van Griensven, A., and Srinivasan, R.: Sediment management modelling in the Blue Nile Basin using SWAT model, Hydrol. Earth Syst. Sci., 15, 807–818, doi:10.5194/hess-15-807-2011, 2011.

Beven, K.: Searching for the Holy Grail of scientific hydrology: $Q_t = (S, R, \Delta t)\, A$ as closure, Hydrol. Earth Syst. Sci., 10, 609–618, doi:10.5194/hess-10-609-2006, 2006.

Bierkens, M. F. P., Finke, P. A., and De Willigen, P.: Upscaling and downscaling methods for environmental research, Kluwer, Dordrecht, 2000.

Blöschl, G. and Sivapalan, M.: Scale issues in hydrological modelling: A review, Hydrol. Process., 9, 251–290, doi:10.1002/hyp.3360090305, 1995.

Blume, T., Zehe, E., and Bronstert, A.: Rainfall – runoff response, event-based runoff coefficients and hydrograph separation, Hydrolog. Sci. J., 52, 843–862, doi:10.1623/hysj.52.5.843, 2007.

Breuer, L., Eckhardt, K., and Frede, H.-G.: Plant parameter values for models in temperate climates, Ecol. Model., 169, 237–293, doi:10.1016/S0304-3800(03)00274-6, 2003.

Brolsma, R. J., Karssenberg, D., and Bierkens, M. F. P.: Vegetation competition model for water and light limitation. I: Model description, one-dimensional competition and the influence of groundwater, Ecol. Model., 221, 1348–1363, doi:10.1016/j.ecolmodel.2010.02.012, 2010.

Bulcock, H. H. and Jewitt, G. P. W.: Spatial mapping of leaf area index using hyperspectral remote sensing for hydrological applications with a particular focus on canopy interception, Hydrol. Earth Syst. Sci., 14, 383–392, doi:10.5194/hess-14-383-2010, 2010.

Burrough, P. A. and McDonnell, R. A.: Principles of Geographical Information Systems, 5th Ed., Oxford University Press, New York, 2004.

Chow, V. T., Maidment, D. R., and Mays, L. W.: Applied Hydrology, McGraw Hill, New York, 1988.

Corradini, C., Morbidelli, R., and Melone, F.: On the interaction between infiltration and Hortonian runoff, J. Hydrol., 204, 52–67, doi:10.1016/S0022-1694(97)00100-5, 1998.

De Jonge, M.: Physically-based hydrological modelling of a subbasin in the Buëch catchment, 57 pp., MSc Thesis, Utrecht University, 2006.

Descroix, L. and Gautier, E.: Water erosion in the southern French alps: climatic and human mechanisms, Catena, 50, 53–85, doi:10.1016/S0341-8162(02)00068-1, 2002.

Dingman, S. L.: Physical Hydrology, 2nd Ed., Prentice Hall, Upper Saddle River, New Jersey, 2002.

Fenicia, F., Zhang, G. P., Rientjes, T., Hoffmann, L., Pfister, L., and Savenije, H. H. G.: Numerical simulations of runoff generation with surface water–groundwater interactions in the Alzette river alluvial plain (Luxembourg), Phys. Chem. Earth, 30, 277–284, doi:10.1016/j.pce.2004.11.001, 2005.

Flügel, W.-A.: Delineating hydrological response units by geographical information system analyses for regional hydrological modelling using PRMS/MMS in the drainage basin of the River Bröl, Germany, Hydrol. Process., 9, 423–436, doi:10.1002/hyp.3360090313, 1995.

Forsythe, W. C., Rykiel, E. J., Stahl, R. S., Wu, H., and Schoolfield, R. M.: A model comparison for daylength as a function of latitude and day of year, Ecol. Model., 80, 87–95, doi:10.1016/0304-3800(94)00034-F, 1995.

Gervais, M., Mkhabela, M., Bullock, P., Raddatz, R., and Finlay, G.: Comparison of standard and actual crop evapotranspiration estimates derived from different evapotranspiration methods on the Canadian Prairies, Hydrol. Process., 26, 1467–1477, doi:10.1002/hyp.8279, 2012.

Giraud, F., Courtinat, B., and Atrops, F.: Spatial distribution patterns of calcareous nannofossils across the Callovian–Oxfordian transition in the French Subalpine Basin, Mar. Micropaleontol., 72, 129–145, doi:10.1016/j.marmicro.2009.04.004, 2009.

Gupta, H. V., Clark, M. P., Vrugt, J. a., Abramowitz, G., and Ye, M.: Towards a comprehensive assessment of model structural adequacy, Water Resour. Res., 48, W08301, doi:10.1029/2011WR011044, 2012.

Harden, C. P. and Scruggs, P. D.: Infiltration on mountain slopes: a comparison of three environments, Geomorphology, 55, 5–24, doi:10.1016/S0169-555X(03)00129-6, 2003.

Hendriks, M. R.: Introduction to Physical Hydrology, Oxford University Press, New York, 2010.

Jana, R. B. and Mohanty, B. P.: A topography-based scaling algorithm for soil hydraulic parameters at hillslope scales: Field testing, Water Resour. Res., 48, W02519, doi:10.1029/2011WR011205, 2012.

Kale, R. V. and Sahoo, B.: Green-Ampt Infiltration Models for Varied Field Conditions: A Revisit, Water Resour. Manage., 25, 3505–3536, doi:10.1007/s11269-011-9868-0, 2011.

Karssenberg, D.: Upscaling of saturated conductivity for Hortonian runoff modelling, Adv. Water Resour., 29, 735–759, doi:10.1016/j.advwatres.2005.06.012, 2006.

Koivusalo, H., Kokkonen, T., Laurén, A., Ahtiainen, M., Karvonen, T., Mannerkoski, H., Penttinen, S., Seuna, P., Starr, M., and Finér, L.: Parameterisation and application of a hillslope hydrological model to assess impacts of a forest clear-cutting on runoff generation, Environ. Modell. Softw., 21, 1324–1339, doi:10.1016/j.envsoft.2005.04.020, 2006.

Kuriakose, S. L., Van Beek, L. P. H., and Van Westen, C. J.: Parameterizing a physically based shallow landslide model in a data poor region, Earth Surf. Proc. Land., 34, 867–881, doi:10.1002/esp.1794, 2009.

Lakshmi, V.: Remote Sensing of Soil Moisture, ISRN Soil Science, 2013, 1–33, doi:10.1155/2013/424178, 2013.

Langhans, C., Govers, G., Diels, J., Leys, A., Clymans, W., Putte, A., Van Den, and Valckx, J.: Experimental rainfall-runoff data:

Reconsidering the concept of infiltration capacity, J. Hydrol., 399, 255–262, doi:10.1016/j.jhydrol.2011.01.005, 2011.

Lazzarotto, P., Stamm, C., Prasuhn, V., and Flühler, H.: A parsimonious soil-type based rainfall-runoff model simultaneously tested in four small agricultural catchments, J. Hydrol., 321, 21–38, doi:10.1016/j.jhydrol.2005.07.038, 2006.

Lee, H., Zehe, E., and Sivapalan, M.: Predictions of rainfall-runoff response and soil moisture dynamics in a microscale catchment using the CREW model, Hydrol. Earth Syst. Sci., 11, 819–849, doi:10.5194/hess-11-819-2007, 2007.

Mango, L. M., Melesse, a. M., McClain, M. E., Gann, D., and Setegn, S. G.: Land use and climate change impacts on the hydrology of the upper Mara River Basin, Kenya: results of a modeling study to support better resource management, Hydrol. Earth Syst. Sci., 15, 2245–2258, doi:10.5194/hess-15-2245-2011, 2011.

Massuel, S., Cappelaere, B., Favreau, G., Leduc, C., Lebel, T., and Vischel, T.: Integrated surface water-groundwater modelling in the context of increasing water reserves of a regional Sahelian aquifer, Hydrolog. Sci. J., 56, 1242–1264, doi:10.1080/02626667.2011.609171, 2011.

Mathys, N. and Klotz, S.: Draix: A field laboratory for research on hydrology and erosion in mountain areas, in Proceedings of the 4th Canadian Conference on Geohazards: From Causes to Management, edited by: Locat, D. D. et S. L. J., Perret, D., Turmel, D., p. 594, Presse de l'Université Laval, Québec, 2008.

McIntyre, N.: Modelling the hydrological impacts of rural land use change: current state of the science and future challenges, in Hydrology for a changing world, 01–07, British Hydrological Society, 2012.

Meng, H., Green, T., Salas, J., and Ahuja, L.: Development and testing of a terrain-based hydrologic model for spatial Hortonian Infiltration and Runoff/On, Environ. Modell. Softw., 23, 794–812, doi:10.1016/j.envsoft.2007.09.014, 2008.

Mileham, L., Taylor, R., Thompson, J., Todd, M., and Tindimugaya, C.: Impact of rainfall distribution on the parameterisation of a soil-moisture balance model of groundwater recharge in equatorial Africa, J. Hydrol., 359, 46–58, doi:10.1016/j.jhydrol.2008.06.007, 2008.

Molnár, D. K. and Julien, P. Y.: Grid-size effects on surface runoff modeling, J. Hydraul. Eng. ASCE, 5, 8–16, 2000.

Moore, R. D.: Introduction to salt dilution gauging for streamflow measurement: part 1, Streamline Watershed Management Bulletin, 7, 20–23, 2004.

Oostwoud Wijdenes, D. J. and Ergenzinger, P.: Erosion and sediment transport on steep marly hillslopes, Draix, Haute-Provence, France: an experimental field study, Catena, 33, 179–200, doi:10.1016/S0341-8162(98)00076-9, 1998.

Oudin, L., Hervieu, F., Michel, C., Perrin, C., Andréassian, V., Anctil, F., and Loumagne, C.: Which potential evapotranspiration input for a lumped rainfall–runoff model? Part 2 – Towards a simple and efficient potential evapotranspiration model for rainfall-runoff modelling, J. Hydrol., 303, 290–306, doi:10.1016/j.jhydrol.2004.08.026, 2005.

Pereira, L. S., Perrier, A., Allen, R. G., and Alves, I.: Evapotranspiration: Concepts and Future Trends, J. Irrig. Drain. E-ASCE, 125, 45–51, doi:10.1061/(ASCE)0733-9437(1999)125:2(45), 1999.

Rawls, W. J., Brakensiek, D. L., and Saxton, K. E.: Estimation of Soil Water Properties, T. ASAE, 25, 1316–1320, 1328, 1982.

Reggiani, P. and Rientjes, T. H. M.: Closing horizontal groundwater fluxes with pipe network analysis: An application of the REW approach to an aquifer, Environ. Modell. Softw., 25, 1702–1712, doi:10.1016/j.envsoft.2010.04.019, 2010.

Reggiani, P., Sivapalan, M., and Majid Hassanizadeh, S.: A unifying framework for watershed thermodynamics: balance equations for mass, momentum, energy and entropy, and the second law of thermodynamics, Adv. Water Resour., 22, 367–398, doi:10.1016/S0309-1708(98)00012-8, 1998.

Reggiani, P., Hassanizadeh, S. M., Sivapalan, M., and Gray, W. G.: A unifying framework for watershed thermodynamics: constitutive relationships, Adv. Water Resour., 23, 15–39, doi:10.1016/S0309-1708(99)00005-6, 1999.

Robichaud, P. R.: Fire effects on infiltration rates after prescribed fire in Northern Rocky Mountain forests, USA, J. Hydrol., 231-232, 220–229, doi:10.1016/S0022-1694(00)00196-7, 2000.

Scurlock, J. M. O., Asner, G. P., and Gower, S. T.: Worldwide Historical Estimates and Bibliography of Leaf Area Index, 1932–2000, Oak Ridge, Tennessee, 2001.

Setegn, S. G., Srinivasan, R., Melesse, A. M., and Dargahi, B.: SWAT model application and prediction uncertainty analysis in the Lake Tana Basin, Ethiopia, Hydrol. Process., 367, 357–367, doi:10.1002/hyp.7457, 2009.

Stone, J. J., Paige, G. B., and Hawkins, R. H.: Rainfall intensiy-dependent infiltration rates on rangeland rainfall simulation plots, T. ASABE, 51, 45–53, 2008.

Troch, P. A.: Hillslope-storage Boussinesq model for subsurface flow and variable source areas along complex hillslopes: 1. Formulation and characteristic response, Water Resour. Res., 39, 1316, doi:10.1029/2002WR001728, 2003.

Van den Putte, A., Govers, G., Leys, A., Langhans, C., Clymans, W., and Diels, J.: Estimating the parameters of the Green-Ampt infiltration equation from rainfall simulation data: Why simpler is better, J. Hydrol., 476, 332–344, doi:10.1016/j.jhydrol.2012.10.051, 2012.

Van Schaik, N. L. M. B., Hendriks, R. F. A., and Van Dam, J. C.: Parameterization of Macropore Flow Using Dye-Tracer Infiltration Patterns in the SWAP Model, Vadose Zone J., 9, 95, doi:10.2136/vzj2009.0031, 2010.

Van Steijn, H. and Hétu, B.: Rain-generated overland flow as a factor in the development of some stratified slope deposits: A case study from the Pays du Buëch (Préalpes, France), Geogr. Phys. Quatern., 51, 3, doi:10.7202/004884ar, 1997.

Vannametee, E., Karssenberg, D., and Bierkens, M. F. P.: Towards closure relations in the Representative Elementary Watershed (REW) framework containing observable parameters: Relations for Hortonian overland flow, Adv. Water Resour., 43, 52–66, doi:10.1016/j.advwatres.2012.03.029, 2012.

Varado, N., Braud, I., Galle, S., Le Lay, M., Séguis, L., Kamagate, B., and Depraetere, C.: Multi-criteria assessment of the Representative Elementary Watershed approach on the Donga catchment (Benin) using a downward approach of model complexity, Hydrol. Earth Syst. Sci., 10, 427–442, doi:10.5194/hess-10-427-2006, 2006.

Vereecken, H., Huisman, J. A., Bogena, H., Vanderborght, J., Vrugt, J. A. and Hopmans, J. W.: On the value of soil moisture measurements in vadose zone hydrology: A review, Water Resour. Res.,

44, 1–21, doi:10.1029/2008WR006829, 2008.

Xia, Y. Q. and Shao, M. A.: Soil water carrying capacity for vegetation: A hydrologic and biogeochemical process model solution, Ecol. Model., 214, 112–124, doi:10.1016/j.ecolmodel.2008.01.024, 2008.

Xu, C.-Y. and Singh, V. P.: Evaluation and generalization of temperature-based methods for calculating evaporation, Hydrol. Process., 15, 305–319, doi:10.1002/hyp.119, 2001.

Yu, Z.: Assessing the response of subgrid hydrologic processes to atmospheric forcing with a hydrologic model system, Global Planet. Change, 25, 1–17, doi:10.1016/S0921-8181(00)00018-7, 2000.

Zehe, E., Lee, H., and Sivapalan, M.: Dynamical process upscaling for deriving catchment scale state variables and constitutive relations for meso-scale process models, Hydrol. Earth Syst. Sci., 10, 981–996, doi:10.5194/hess-10-981-2006, 2006.